UNIVERSIDADE D
COIMBRA

Rita Ferreira Mendes

OPTIMIZATION OF A LINEAR ROBOT FOR PIPETTING AND ELIMINATION OF MICROORGANISMS USING COLD ATMOSPHERIC PLASMA

Dissertação no âmbito do Mestrado Integrado em Engenharia Biomédica no ramo de Instrumentação Biomédica orientada pelo Professor Doutor Pedro Mariano Simões Neto e pelo Professor Doutor Francisco José Santiago Fernandes Amado Caramelo e apresentada ao Departamento de Engenharia Mecânica da Faculdade de Ciências e Tecnologia da Universidade de Coimbra.

Outubro de 2021

UNIVERSIDADE D
COIMBRA

Rita Ferreira Mendes

OPTIMIZATION OF A LINEAR ROBOT FOR PIPETTING AND ELIMINATION OF MICROORGANISMS USING COLD ATMOSPHERIC PLASMA

Dissertação no âmbito do Mestrado Integrado em Engenharia Biomédica no ramo de Instrumentação Biomédica orientada pelo Professor Doutor Pedro Mariano Simões Neto e pelo Professor Doutor Francisco José Santiago Fernandes Amado Caramelo e apresentada ao Departamento de Engenharia Mecânica da Faculdade de Ciências e Tecnologia da Universidade de Coimbra.

Outubro de 2021

This work was developed in collaboration with:

CEMMPRE - Centre for Mechanical Engineering, Materials and Processes

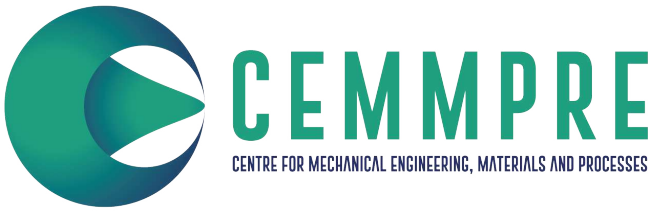

CNC - Centre for Neuroscience and Cell Biology

Coimbra Institute for Clinical and Biomedical Research

Faculty of Medicine of University of Coimbra, Portugal

Faculty of Sciences and Technology of University of Coimbra, Portugal

Agradecimentos

Com a apresentação do trabalho desenvolvido que representa o fim dos meus estudos académicos, não poderia deixar de agradecer a todas as pessoas que fizeram parte desta etapa da minha vida.

Em primeiro lugar, quero agradecer aos meus orientadores, Professor Doutor Pedro Neto e Professor Doutor Francisco Caramelo, pela oportunidade de desenvolver este projeto e por todo o apoio, dedicação e disponibilidade ao longo do mesmo. Obrigada pela orientação durante este ano desafiante e por todos os conselhos e conhecimentos transmitidos que possibilitaram a concretização deste projeto!

Agradeço aos meus colegas do Laboratório de Robótica Colaborativa da Universidade de Coimbra, por todo o apoio, dicas e, acima de tudo, pela boa disposição constante! Um agradecimento especial ao Diogo por toda a ajuda e tempo disponibilizado. Agradeço também a todos os colegas do grupo de Microbiologia Médica e do Instituto de Biofísica da Faculdade de Medicina da Universidade de Coimbra pela colaboração, ajuda e disponiblidade que contribuíram para este trabalho.

A todos os meus amigos, agradeço por me apoiarem e tornarem os meus dias mais felizes, sem vocês esta jornada teria sido muito mais difícil. Mariana e Rafaela, obrigada por todos os desabafos, risos e histórias para contar, levo-vos comigo para a vida. Adriana e Daniela, obrigada por estarem sempre lá para me ouvir e obrigada por esta amizade que é das melhores coisas que tenho na vida.

Agradeço a Coimbra, por ter sido a cidade que tão bem me acolheu durante os últimos cinco anos e que me fez sempre sentir em casa.

Agradeço à minha família, pelo apoio incondicional, por acreditarem no meu potencial e por me ajudarem a ultrapassar os dias mais difíceis, mesmo sem se aperceberem. Aos meus pais, obrigada por todas as oportunidades que me deram ao longo da vida, por me incentivarem sempre a conquistar os meus objetivos, por me apoiarem nas minhas decisões e por me fazerem acreditar em mim. Nunca vos poderei agradecer o suficiente por tudo o que fazem diaramente por mim.

O meu sincero agradecimento a todos!

"All progress takes place outside the comfort zone."

Michael John Bobak

Abstract

The quality of laboratory work has been significantly improved by systems that automatize manual repetitive tasks. The possibility to automatize clinical laboratory techniques allows the researchers to focus on high value-added procedures and insures fewer human errors in these tasks. Therefore, the automation technology improves the productivity of medical investigation laboratories by reducing the time spent on repetitive tasks and increasing their reproducibility.

At the Biophysics Institute of the Faculty of Medicine of the University of Coimbra, the application of Cold Atmospheric Plasma (CAP) to culture cells is performed by a recently adapted linear robot, which showed a reduction in the variability of results and a decrease in the technique duration, when compared with the previous manual system. The CAP irradiation has been analyzed, especially on its lethality in tumor cells, in order to study its potential in cancer treatment. The results obtained from the studies with CAP, already performed at the Biophysics Institute of the University of Coimbra, revealed a high specificity and lethality in tumor cells associated with maintenance of the integrity of normal cells.

Nowadays, healthcare-associated infections (HAIs) represent one of the most relevant problems in health area, with bacteria resistant to antibiotics as a major cause of HAIs worldwide. Therefore, one of the main goals of the present project was to extend the study of the effect of CAP irradiation to microorganisms, in order to analyze the potential of CAP in decontamination and infections eradication.

Furthermore, the pipetting technique when performed manually represents a highly repetitive and time-consuming task that leads to a possibility of human errors and a low reproducibility. The continuous sequence of this technique also exposes the laboratory technician to ergonomic hazards in the long term and provides inappropriate management of the laboratory working time. Therefore, the second main goal of this dissertation was to fully automatize the pipetting technique, by adapting the linear robot already in use at the Biophysics Institute of the University of Coimbra.

Regarding the first main goal of the present project, relative to the application

of CAP, the assays were performed in bacterial and fungal strains with exposure times of 30, 60 and 120 seconds. The CAP effect was not so clear for the two yeasts tested, *Candida albicans* and *Candida parapsilosis*, and for the fungus *Alternaria alternata* as it was for the rest of the microorganisms tested. However, the bactericidal effect was achieved in bacteria *Pseudomonas aeruginosa* and *Staphylococcus aureus*, and was reached a reduction of approximately 99% of the initial population of the *Escherichia coli*.

Furthermore, the results were also interesting relative to the potential of CAP as an antimicrobial treatment for the dermatophytes *Trichophyton rubrum* and *Trichophyton mentagrophytes* and for the filamentous fungus *Aspergillus fumigatus*, which is one of the most difficult fungi that affect the human species. Therefore, the obtained results promote further research to understand potential of CAP as an antimicrobial treatment since the performed irradiation assays revealed a growth inhibition in most microorganisms tested.

For the automatization of the pipetting technique, an end-effector was developed according to the requirements, with a mechanism of actuation based on a racks and pinion system moved by a servo motor. To execute this specific application, the motor is controlled by three different commands that can be triggered by the reception of a signal from the robotic system, depending on its duration. To validate the final robotic system were performed several tests.

The obtained results showed that the developed system of automatization performs the pipetting technique without human intervention, which increases the productivity of researchers in the laboratory, reduces the long-term impact on their musculoskeletal system and allows a higher reproducibility. Besides, the developed system highlights the potential of the interaction between human and robot in clinical environment and the modularity of the robot improves its rentability and utility in the laboratory.

Keywords: Robotics, Automatizing, Pipetting, Cold Atmospheric Plasma, Infections.

Resumo

A qualidade do trabalho de laboratório tem sido significativamente melhorada por sistemas que automatizam tarefas manuais repetitivas. A possibilidade de automatizar técnicas de laboratórios clínicos permite que os investigadores se foquem em procedimentos de alto valor adicionado e garante menos erros humanos nessas tarefas. Portanto, a tecnologia de automatização melhora a produtividade dos laboratórios de investigação médica ao reduzir o tempo gasto em tarefas repetitivas e ao aumentar a sua reprodutibilidade.

No Instituto de Biofísica da Faculdade de Medicina da Universidade de Coimbra, a aplicação de Plasma Frio Atmosférico (PFA) em culturas de células é desempenhada por um robot linear recentemente adaptado, que demonstrou uma redução na variabilidade dos resultados e uma diminuição na duração da técnica, quando comparado com o sistema manual anterior. A irradiação de PFA tem sido analisada, especialmente sobre a sua letalidade em células tumorais, de forma a estudar o seu potencial no tratamento do cancro. Os resultados obtidos dos estudos com PFA, anteriormente realizados no Instituto de Biofísica da Universidade de Coimbra, revelaram uma elevada especificdade e letalidade em células tumorais associadas a uma manutenção da integridade de células normais.

Atualmente, as infeções associadas aos cuidados de saúde (IACS) representam um dos maiores problemas na área da saúde, sendo que as bactérias resistentes aos antibióticos constituem a sua maior causa em todo o mundo. Portanto, um dos principais objetivos do presente projeto consistiu em alargar o estudo do efeito da irradiação de PFA a microrganismos, de forma a analisar o potencial do PFA na descontaminação e no combate de infeções.

Por outro lado, a técnica de pipetagem quando desempenhada manualmente representa uma tarefa bastante repetitiva e demorada que leva à possibilidade de erros humanos e baixa reprodutibilidade. A sequência contínua desta técnica também expõe o técnico de laboratório a riscos ergonómicos a longo prazo e origina uma gestão desapropriada do tempo de trabalho laboratorial. Portanto, o segundo principal objetivo desta dissertação consistiu em automatizar completamente a técnica

de pipetagem, adaptando o robot linear já em utilização no Instituto de Biofísica da Universidade de Coimbra.

Quanto ao primeiro objetivo do presente projeto, relativo à aplicação de PFA, os ensaios foram realizados em bactérias e fungos com tempos de exposição de 30, 60 e 120 segundos. O efeito do PFA não foi tão claro para os dois tipos de leveduras testadas, *Candida albicans* e *Candida parapsilosis*, e para o fungo *Alternaria alternata*, como foi para os restantes microorganismos testados. No entanto, o efeito bactericida foi atingido nas bactérias *Pseudomonas aeruginosa* e *Staphylococcus aureus*, e foi alcançada uma redução de aproximadamente 99% da população inicial da bactéria *Escherichia coli*.

Para além disso, os resultados foram também interessantes relativamente ao potencial do PFA como um tratamento antimicrobiano para os dermatófitos *Trichophyton rubrum* e *Trichophyton mentagrophytes* e para o fungo filamentoso *Aspergillus fumigatus*, que é um dos fungos mais complicados que afetam a espécie humana. Portanto, os resultados obtidos promovem uma pesquisa futura para entender o potencial do PFA como um tratamento antimicrobiano, uma vez que os ensaios de irradiação realizados revelaram uma inibição de crescimento na maioria dos microrganismos testados.

Para a automatização da técnica de pipetagem, foi desenvolvido um *end-effector* de acordo com os requisitos, com um mecanismo de atuação baseado num sistema de pinhão e cremalheiras, movido por um servomotor. Para executar esta aplicação específica, o motor é controlado através de três comandos diferentes que podem ser ativados pela recepção de um sinal do sistema robótico, dependendo da sua duração. Para validar o sistema robótico final foram realizades vários testes.

Os resultados obtidos mostraram que o sistema de automatização desenvolvido realiza a técnica de pipetagem sem intervenção humana, o que aumenta a produtividade dos investigadores no laboratório, reduz o impacto a longo prazo no sistema músculo-esquelético dos mesmos e permite uma maior reprodutibilidade. Para além disso, o sistema desenvolvido enaltece o potencial da interação entre humano e robot em ambiente clínico e a modularidade do robot aumenta a sua rentabilidade e utilidade no laboratório.

Palavras-chave: Robótica, Automatização, Pipetagem, Plasma Frio Atmosférico, Infeções.

Contents

List of Figures

List of Tables

List of Abbreviations

CAD Computer-Aided Design. 29, 36, 39
CAP Cold Atmospheric Plasma. v, vi, x, xii, 1, 2, 3, 8, 9, 10, 11, 12, 49, 53, 57, 60, 61, 62, 63, 65, 66
CFU Colony Forming Unit. xii, 51, 52, 54, 55, 60
CLSI Clinical & Laboratory Standards Institute. 52
CNC Centre for Neuroscience and Cell Biology. 51

DNA Deoxyribonucleic Acid. 8, 9, 10, 11
DOF Degrees of Freedom. 26
DSA Dual Solenoid Actuator. xi, 20, 21

FEA Finite Element Analysis. 37
FMUC Faculty of Medicine of the University of Coimbra. 51

HAI Healthcare-Associated Infection. v, xiii, 2, 5, 6

IACS Infeções Associadas a Cuidados de Saúde. vii
IDE Integrated Development Environment. 45

MIC Minimum Inhibitory Concentration. 52, 54, 60
MRSA Meticillin-Resistant *Staphylococcus Aureus*. 5
MSD Musculoskeletal Disorder. 2

NaCl Sodium Chloride. 51

PFA Plasma Frio Atmosférico. vii, viii
PLA Polylactic Acid. 11, 37, 39

RNS Reactive Nitrogen Species. 8, 10
ROS Reactive Oxygen Species. 8, 10

STL Standard Tessellation Language. 39

UTS Ultimate Tensile Strength. 38

UV Ultraviolet. 7, 8, 10

VBNC Viable but non-culturable. 10
VRE Vancomycin-Resistant *Enterococcus*. 5

WHO World Health Organization. 5

YPD Yeast Extract Peptone Dextrose. 51

Chapter 1

Introduction

This chapter provides a brief explanation of this thesis proposal which includes its context in section 1.1 and the general approach to its problem and motivation in section 1.2. The proposed approach to achieve the objectives is found in section 1.3. Finally, the structure of the document is presented in the last section of this chapter.

1.1 Context

The quality of laboratory work has been significantly improved by systems that automatize manual tasks representative of routine activities. The possibility to automatize clinical laboratory techniques previously performed by human labour, such as pipetting of samples, measurements, and preparations weighing, allows the laboratory operators to focus on higher value procedures and insures fewer human errors in these tasks. Therefore, the automation technology improves the productivity of medical investigation laboratories by reducing the time spent on repetitive tasks [1].

At the Biophysics Institute of the Faculty of Medicine of the University of Coimbra, the application of Cold Atmospheric Plasma (CAP) has been analyzed, especially on its lethality in tumor cells, in order to study its potential in cancer treatment. For some time, the exposure of cell cultures to CAP was a fully manual performed procedure and it was a repetitive and time-consuming laboratory technique, prone to human error and with low reproducibility.

Therefore, a linear robot was recently adapted to the technique of CAP irradiation. The obtained results demonstrated a reduction of the technique duration which allows the researchers' work in the laboratory to be more efficient. The support of the robotic system in CAP irradiation also showed a reduction in the variability of results, which can be translated into a better precision in the CAP application comparing with the manual system [2].

Accordingly, this robot allows laboratory workers to focus on high value-added investigation tasks instead of monotonous and repetitive tasks, such as the pipetting technique or the application of CAP. Furthermore, the use of this robot ensures a higher reproducibility, allowing to maintain the same conditions and perform the various procedures equally, which leads to greater control and predictability of the entire process.

Nowadays, healthcare-associated infections (HAIs) represent one of the most relevant problems in health area. In clinical environments, many aspects are significantly influenced by HAIs, such as the safety of both patients and healthcare workers [3].

Bacteria resistant to antibiotics are a major cause of HAIs worldwide and, therefore, contribute to an alarming healthcare problem, which has been aggravated by the presence of multiresistant organisms. Infections, particularly those caused by multiresistant bacteria, significantly increase mortality, morbidity, and costs in the health area [4].

1.2 Problem and Motivation

The results obtained from the studies of the application of CAP performed at the Biophysics Institute of the University of Coimbra, revealed a high specificity and lethality in tumor cells associated with maintenance of the integrity of normal cells. Therefore, this project intends to extend the study of the effect of CAP irradiation to microorganisms, in order to analyze the potential of CAP in decontamination and infections eradication.

Manual pipetting implies a repetitive motion of the thumb and the prolonged activity of this movement may lead to an overuse of the muscles/tendons and articular joints of the thumb, hand and wrist. Highly repetitive manual techniques are related to the development of upper extremity musculoskeletal disorders (MSDs), being tendinitis one of the most common associated syndromes [5]. Accordingly, the continuous sequence of this task in the long term exposes the laboratory technician to ergonomic hazards.

Furthermore, this highly repetitive task being performed manually, leads to a possibility of human errors and a low reproducibility, since it is almost impossible for humans to pipette over several times with a constant rate of aspiration or dispensing. Besides the influence on the results, the manual performance of this technique also provides inappropriate management of laboratory working time, which results in an avoidable economic expense on laboratory bills. In order to optimize researchers'

laboratory work and to reduce the impact on their musculoskeletal system, this project also aims to automatize the pipetting technique.

1.3 Objectives

This project's objectives consisted in optimize the cartesian robot, already in service at the Biophysics Institute of the Faculty of Medicine of the University of Coimbra, and adapt it to the application of CAP in microorganisms, reducing setup times and increasing its flexibility.

This project also aimed to perform *in vitro* studies based on bacterial and fungal cultures and to evaluate the effect of CAP irradiation in these microorganisms.

In order to automatize the pipetting technique, this task was studied in detail, identifying the requirements of the approach to be developed. The final system has to be validated by performing tests, both with manual pipetting and with automated pipetting.

The main focus is to develop a low-cost system able to automate both of these processes, that is reprogrammable and easy and intuitive to use by any person, without being required any robotics knowledge. Besides, the robot should be modular, being possible to change the end-effector according to the procedure to perform, whether the pipetting technique, the application of CAP, or any other technique.

1.4 Thesis Structure

The present document is divided into six chapters that describe the work developed throughout the realization of this dissertation.

Chapter 1 introduces the study by contextualizing the problem and referring the main goals of this project. **Chapter 2** presents the literature review concerning infections, CAP, actuation technologies and robotics applied to the laboratory environment, namely to the pipetting technique.

Chapter 3 includes all the stages pursued in the work of automatizing the pipetting technique, from the prototype of the system to the actual manufacturing and control of the final end-effector. **Chapter 4** describes the procedures performed for the application of CAP in microorganisms.

Chapter 5 contains the analysis of the validation tests of the developed robotic system and also presents the discussion of the results of the application of CAP in microorganisms. Lastly, **chapter 6** presents the conclusion of the developed work and proposes suggestions for the future work.

Chapter 2

Literature Review

2.1 Microbial Infections

Nowadays, healthcare-associated infections (HAIs) represent one of the most relevant problems in health area that can significantly influence the safety of both patients and healthcare workers [3]. Antibiotic-resistant bacteria are one of the major causes of HAIs around the world. Infections, particularly those caused by multiresistant organisms, have become an alarming healthcare problem since they significantly increase mortality, morbidity, and costs in the health area [4].

According to the World Health Organization (WHO), there are approximately 4.5 million patients affected by HAIs per year in Europe, whose account for an estimate of 100000 deaths per year [6]. Several studies already showed that a large percentage of HAIs could be prevented by decontamination of the hospital environment and, therefore, the transmission of dangerous pathogens to patients could be avoided [3].

High-touch surfaces of the hospital environment may get contaminated with organisms that cause common HAIs, including the gram-positive bacteria meticillin-resistant *Staphylococcus aureus* (MRSA), vancomycin-resistant *Enterococcus* (VRE) spp. and *Clostridium difficile*, and the multiresistant gram-negative bacteria, *Escherichia coli* and *Pseudomonas aeruginosa* [6]. Besides the types of bacteria mentioned, several fungi can also persist on surfaces, including the yeasts *Candida albicans* and *Candida parapsilosis* [7].

These pathogens can survive in viable form for long periods in surfaces frequently involved in contamination, including floors, linen, bedrails, mattresses, patients' clothing and call buttons. This long-lasting presence of organisms responsible for HAIs in the hospital environment represents a transmission risk for both patients and healthcare professionals due to physical contact with microbes or through airborne contaminants [6]. The survival time of the microorganisms mentioned are

presented in Table 2.1.

Table 2.1: Survival time of principal microorganisms causing HAIs on dry inanimate surfaces (adapted from [3, 7]).

Microorganism	**Type of microorganism**	**Duration of persistence**
Gram-positive bacteria	*Staphylococcus aureus*	7 days - 7 months
	Clostridium difficile	5 months
	Enterococcus spp.	5 days - 4 months
Gram-negative bacteria	*Escherichia coli*	1.5 hours - 16 months
	Pseudomonas aeruginosa	6 hours - 16 months
Fungi	*Candida albicans*	1 day - 120 days
	Candida parapsilosis	14 days

Overall, gram-negative bacteria present a longer persistence than gram-positive bacteria, which is frequently improved by humid conditions for most bacteria. Regarding fungi, *Candida albicans*, which represents the most important fungal pathogen and the type of yeast with longer persistence time, can survive until 4 months on surfaces. The high humidity also influences positively to the survival of yeasts. Since the duration of persistence of the mentioned pathogens on inanimate surfaces is relatively high, an adequate disinfection of surfaces in areas intended for patient care is recommended to reduce the transmission risk [7].

Besides the decontamination of the hospital environment, the eradication of specific pathogens in infections, without affecting the normal tissue cells, remains a challenge in medicine. Despite already existing a range of antimicrobial treatments available, combating infections is still a threatening process due to the increasing microbial resistance to antibiotics. The search for better antimicrobial treatments, especially not subject to resistance evolution, represents a crucial condition to succeed in combating infections [8].

Beyond the microorganisms responsible for infections already mentioned, the eradication of dermatophytes, which represent a group of filamentous fungi, also present interest in medicine. The dermatophytes are prone to infect tissues rich in keratin, including skin, hair and nails, and the infections caused by them, denominated dermatophytoses, are recognized as the most common fungal infections, affecting between 20% and 25% of the population worldwide. Between the dermatophytes, *Trichophyton rubrum* is considered the most predominant superficial fungus and agent of skin and nail dermatophytoses, being followed by *Trichophyton mentagrophytes* [9].

Invasive fungal diseases belong to the most severe complications in immunocompromised individuals. *Aspergillus fumigatus* is an opportunistic filamentous fungus and currently represents the most common cause of invasive fungal disease in this high-risk population [10]. Besides, this fungus capacity of adapting and proliferating in hostile environments allows its resistance against human defenses. This resistance leads to a longer survival time and consequently to a lung infection, considered one of the most devastating in terms of mortality and morbidity [11].

Regarding plant infections, *Alternatia* spp. are described as responsible of diseases in more than 400 species. More specifically, *Alternaria alternata*, a filamentous fungus, represents a potent contaminator of both food and feed. Despite the associated health problems usually represent only long-term effects, the contamination from *A. alternata* may lead to several mycotoxicoses, which are human or animal diseases due to the consumption of foods contaminated with fungi, and in the worst-case can even end with cancer. Therefore, the decontamination of food also shows interest in health area [12].

2.2 Cold Atmospheric Plasma

2.2.1 Plasma Classifications

Plasma represents the fourth essential state of matter, added to the three most commonly encountered ones, solid, liquid, and gas. A solid when heated transforms into a liquid and when a liquid is heated, it becomes a gas [13].

Plasma is generated by adding energy, in form of heat or electromagnetic fields, to a neutral gas, which becomes an ionized gas. The plasma is composed of charged species and reactive chemical species, such as ions, electrons, neutral molecules, and atoms. During plasma generation, there is emission of radiation in the ultraviolet (UV), visible and near-infrared regions [13].

Plasma can be classified based on temperature, into thermal and non-thermal, or according to gas pressure, into low-pressure and atmospheric pressure plasma. While thermal or hot plasma is fully ionized, non-thermal or cold plasma is only partially ionized, which means that besides ions and electrons, it also has neutral atoms. In thermal plasma, all particles, including electrons, atoms and ions, have the same temperature, establishing a thermal equilibrium. Non-thermal plasma is generated by applying a high frequency alternating field, such as as an electromagnetic field, and its particles are not in thermal equilibrium [14].

2.2.2 Characteristics of Cold Atmospheric Plasma

In the laboratory, non-thermal or cold plasma can be created by applying an external energy source to a gas. By using different gases, cold plasma can be achieved at different pressures, low or atmospheric [14].

CAP is a cold plasma with a temperature close to ambient temperature and is constituted by negative and positive ions. CAP emits UV radiation and its discharge may form reactive species, which can induce cell death or cell proliferation, according to their concentration [2].

In particular, reactive oxygen species (ROS) and reactive nitrogen species (RNS) are biologically relevant since many of them behave as second messengers or are involved in signalling pathways. These reactive species are created when plasma discharge happens in or with air. ROS and RNS, when transferred to the target cells can induce oxidative stress in them [15].

The reactive species formed in plasma discharge, when in large concentrations, can induce Deoxyribonucleic Acid (DNA) damage in the target cells, which may result in apoptosis or other forms of cell death [2]. The ability to kill cells is being explored in several applications, including in the inactivation of microorganisms and in the induction of death in cancer cells [15].

2.2.3 Biomedical Applications of CAP

Depending on the dose or time of CAP irradiation, it can be useful for different applications. While low-dose or short-time plasma treatment can induce cell stimulation, repair of damaged DNA, rapid sterilization or promotion of proliferation and migration, high-dose or long-time plasma treatment can cause cell death by apoptosis or lethal cell damage, such as irreversible DNA damage, stop of cell proliferation and cell cycle arrest [16].

Therefore, CAP is a versatile emerging technique in the biomedical field with a vast range of applications, including disinfection, tissue regeneration, blood coagulation, wound healing, and cancer treatment. Since CAP temperature is close to ambient temperature, as already mentioned, its application is allowed on heat-sensitive biological matter, like living tissue, being adequately safe for human treatment [15].

Application of CAP in Wound Healing

Wound healing is a complicated process, given the complexity of its multiple phases, inflammatory, proliferative, and remodeling, which are easily affected by

disturbances, both internal and external. These disturbances may lead to chronic or nonhealing wounds [16].

The majority of cutaneous wounds is colonized with bacteria and chronic or nonhealing wounds shows persistence of bacteria and biofilm formation, which damage the wound healing process [16].

The typical use of antimicrobial agents in wound healing to damage the colonizing microorganisms is limited by the development of multiresistant bacteria and the hypersensitivity to antibiotics [16].

As an alternative, CAP can effectively inactivate infectious microorganisms without developing resistance to plasma damage or allergic reactions on the skin, and, consequently, promotes wound healing [16].

Application of CAP in Decontamination and Sterilization

Studies have demonstrated the efficiency of CAP in the inactivation of fungi and bacteria. The application of CAP in these microorganisms results in DNA damages that are not reversible. On the other hand, eukaryotic cells can easily overcame these lesions, which shows CAP selectivity to eliminate bacteria and fungi. Therefore, CAP is useful for applications as decontamination of surfaces and sterilization of living tissues [2].

The potential of CAP in sterilization is wide-ranging, since it is useful in several fields, such as medicine, dentistry and agriculture. In medicine and dentistry, CAP can be used for sterilization or disinfection of medical and dental devices. These instruments, when contaminated with pathogens, may induce secondary infections. This technology could also be applied as decontamination system in desks, beds, and floors in clinical environments in order to prevent hospital-acquired infections. In the agricultural field, CAP can be used in disinfection of food, equipment, packaging materials, and agricultural sources, as fertilizer, seeds, water, and soil [13].

CAP technology is advantageous over current decontamination methods used in hospital environments since it shows a limited toxicity and a non-thermal nature, representing minimal risk to both healthcare staff and patients [6].

Application of CAP in Infection Control

As already mentioned, CAP has shown potential as an antimicrobial treatment and presents particular interest for combating infections, which, despite the range of current treatments available, is still challenging due to the increasing microbial resistance [8].

The methods already developed to eradicate pathogenic bacteria for infection control include antibiotics, UV, heat, pressure, antimicrobial nanoparticles, antibacterial peptides and chemical disinfection [8].

In comparison with these common antibacterial technologies, the application of CAP presents advantages as short treatment time, high efficiency, limited side effects and local application [8].

CAP treatment can affect bacterial cells via three different mechanisms, following described. This technology can directly permeabilize the cell wall or membrane leading to a posterior leakage of the cellular components, critically damage intracellular proteins with ROS and RNS generation or induce direct chemical DNA damage. On the other hand, short-time exposure to CAP can induce bacterial response mechanisms, such as a viable but non-culturable (VBNC) state or cell refuge formation [8].

CAP treatment, when used as an antibacterial method, performs multiple modes of action, being unlikely to promote resistance in bacteria. Furthermore, CAP application, with dose and time controlled, can eradicate pathogenic bacteria without damaging mammalian tissue cells. Therefore, application of CAP represents a cutting-edge antimicrobial treatment [8].

Application of CAP in Cancer Treatment

In oncology, CAP is emerging as a promising alternative for tumor treatment.

Current treatments present non-selectivity to the malignant cells, since they also damage the adjacent normal cells, and commonly lead to resistance of the tumor cell to the therapy. Therefore, a therapy based on CAP arises from the challenge of researching a more effective tumor treatment. The application of CAP has shown to affect several cellular processes, inducing different effects on cells [17].

Tumor cells have increased proliferative activity that can be caused by the higher amounts of ROS and RNS that they produce, which makes them more susceptible to oxidative stress caused by plasma. The CAP application increases, even more, the levels of these reactive species, leading to a lethal level and posterior apoptosis [16, 18].

Another possible effect of CAP in cells is related to the UV radiation produced in its discharge. This radiation is absorbed by the cells, affecting directly the DNA and inducing disturbances in cell balance, which later leads to cell death [2].

CAP discharge also generates electric fields that can induce apoptosis by affecting cell membrane permeability, mitosis, DNA structure and synthesis, cell growth,

and calcium permeability through voltage-sensitive calcium channels [2, 17]

In terms of selectivity, the application of CAP mainly affects cells of the target tissue that are in the DNA replication phase, which is recurrent for most cancer cells, since they have a faster duplication time than normal cells. Moreover, studies suggest that, if duration and dose of the treatment are appropriate, CAP can selectively kill cancerous cells with no critical effects on adjacent normal cells [16].

2.2.4 Robotic System for Application of CAP

CAP generating devices can be divided into direct, indirect, and hybrid devices, depending on the characteristics of the electrode configuration and the use mode for treatment.

In direct plasma devices, the target tissue acts as an electrode, integrating the electric circuit, which allows direct contact between the produced species and the tissue surface. In these sources, it is required to establish a constant gas space between the tissue and the electrode.

In indirect plasma devices, plasma generation involves two electrodes and subsequent transport to the target tissue through a gas flow. These devices include a wide range of configurations, varying in size, energy, and type of gas.

In hybrid plasma devices, the technique of plasma production of direct sources is combined to the essentially current-free property of indirect sources [17].

A device capable of generating CAP by an indirect source was designed and built at the Biophysics Institute. The intrinsic characteristics of the device will not be presented in this thesis due to intellectual property reasons [2].

The CAP produced in this device is then conducted in electrodes for its application in samples. The Figure 2.1 illustrates the robotic system developed to perform the CAP application. The end-effector holds the needles which are connected to crocodile electric plugs, responsible for plasma and current conduction. In the table of the robotic system, the well plate is fixed with a support made of polylactic acid (PLA) [2].

2.3 Robotics in Laboratory Environment

Nowadays, robotics is broadly integrated into various domains, especially in industry, where repetitive procedures are common tasks. Robotic systems can be incorporated into several healthcare areas, including the clinical laboratory, taking the industry as a model [19].

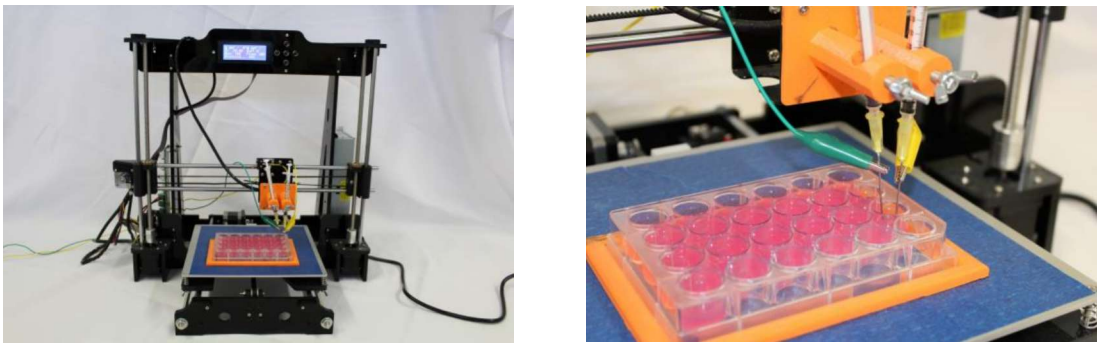

(a) **(b)**

Figure 2.1: Robotic system developed to perform CAP application. In (a) is represented the total system and in (b) is visible the CAP application in detail (adapted from [2]).

Despite the idea of using robotic systems to reproduce human activity is already thousands of years, robots were only introduced in medicine about 30 years ago [20].

In recent years, collaborative robots have increasingly been developed for different automation applications, more specifically in the industry area [21]. The collaboration between humans and robots in the same workspace requires a safe system, able to immediately react to unexpected events with precision.

The evolution of robotics has attracted the attention of scientific and technological community and new robotic solutions are constantly being developed to efficiently perform human tasks [22]. Automation is revolutionizing clinical laboratories, more specifically chemistry and hematology ones, by increasing capacity and improving standardization while reducing turnaround time and human error [23].

Furthermore, robotics represents a serious advantage in radiochemistry by avoiding human exposure to high doses of radiation. Besides, the use of robots in clinical laboratories ensures the operators' safety when dealing with highly lethal viruses. In addition, the high precision of robots increases the reliability of the performed procedures, as in surgery.

In the laboratory environment, repetitive tasks, such as pipetting, are recurrent and highly time-consuming procedures, which results in a low rentability of researchers working time. Besides that, the manual performance of these techniques is prone to human errors, which can compromise their reproducibility, and represents a risk on the researchers' musculoskeletal system. Therefore, robotic systems have been introduced in medical laboratories to perform these repetitive procedures and to establish a collaboration with laboratory technicians.

The application of robots in clinical laboratories, as in the general healthcare

field, implies safe robotic systems, able to collaborate with the researchers and to interact with the surrounding environment.

2.3.1 Pipetting technique

Pipettes are used to measure and transfer precise volumes of liquids and constitute recurrent instruments in laboratories that help researchers in their daily work. Currently, is possible to find a wide choice of pipettes, differentiated from the working principles to the volume ranges.

Working Principle of Pipettes

Pipettes can have two working principles that are recommended for different applications. In order to choose the right pipette for a specific application, it is necessary to analyse the volume to transfer and the physical properties of the sample. The air-displacement pipettes are used for aqueous samples and for general laboratory work while the positive-displacement are recommended for non-aqueous samples, including viscous, hazardous, and corrosive samples [24].

The Figure 2.2 represents a diagram of air-displacement pipettes used by Gilson in order to explain the function of the several parts of a pipette.

The positive-displacement pipettes of the same brand are similar but in place of only a disposable tip, there are disposables capillary and piston and the push button is the only one that adjusts the volume, there is no fine volume adjustment ring. Furthermore, instead of having a specific ejector button, the push button performs that function when pressed down to the last stop position, ejecting both capillary and piston without hand contact.

The air-displacement pipettes have a cushion of air between the sample and the piston, which is inserted inside the lower part of the pipette. By pressing the push button, the piston moves down to let air out and the volume of air displaced by the piston is equivalent to the volume of liquid aspirated. In positive-displacement pipettes, there is direct contact between the sample and the disposable piston, which is not integrated into the pipette but part of the tip. Since there is no expansion or contraction due to elastic air cushion, the aspiration force is not affected by the physical properties of the sample, remaining constant. Therefore, it is possible to use positive-displacement pipettes with viscous and high-density samples, such as blood and glycerol [24].

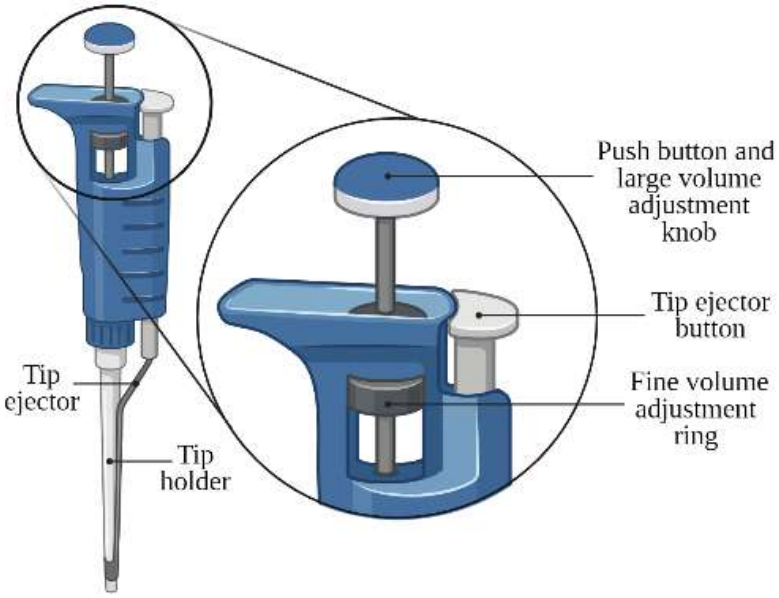

Figure 2.2: Diagram of air-displacement pipette (created with biorender.com).

Pipetting modes

With air-displacement pipettes, it is possible to perform the pipetting technique following two different modes, while with positive-displacement pipettes is available only one mode. The forward mode is considered the standard pipetting and is possible with both pipette types. It is preferably recommended for aqueous samples. The reverse technique is only performed by air-displacement pipettes and is mainly used for dispensing viscous liquids or with a high tendency to foam. This mode is also recommended for the transfer of small volumes. The two modes for pipetting are represented in Figure 2.3 and described below [24, 25].

In case of forward mode pipetting, the operator performs the steps listed below:

1. Press the push button to the first stop position, while holding the pipette in a nearly vertical position.

2. With the push button pressed, dip the tip into the liquid. Consider the immersion depth of the tip to avoid affecting the accuracy of the procedure. Smoothly and slowly release the button to the rest position to aspirate the set volume of the sample.

3. In order to dispense the liquid into the receiving reservoir, establish an angle, from 10^{o} to 45^{o}, between the pipette tip and the inside wall of the vessel. Gently depress the button to the first stop position.

4. In case of remaining liquid at the tip after step 3, press the button to the

second stop position to totally empty the tip.

5. Release the button to the rest position.

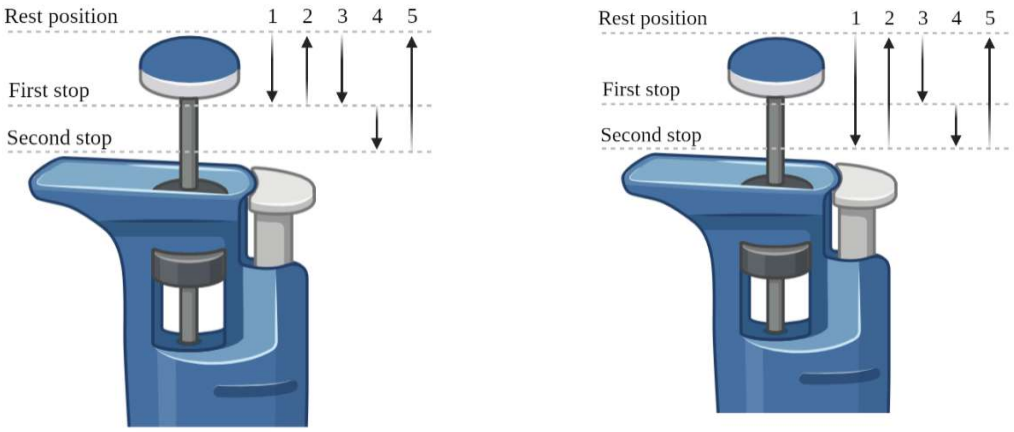

(a) **(b)**

Figure 2.3: Schematic diagram of the two pipetting modes with an air-displacement pipette (created with biorender.com). In (a) is represented the forward mode pipetting and in (b) is shown the reverse mode pipetting.

In case of reverse mode pipetting, the operator performs the following steps:

1. Press the push button to the second stop position, while holding the pipette in an almost vertical position.

2. With the button pressed, immerse the pipette tip in the liquid. Consider the immersion depth of the tip to avoid affecting the accuracy of the procedure. Allow the button to slowly move up to the rest position to aspirate the selected volume of the solution.

3. To dispense the liquid, place the tip at an angle, from 10^{o} to 45^{o}, against the inside wall of the receiving container and smoothly depress the button to the first stop position.

4. The remaining liquid at the tip after step 3 should not be dispensed in the receiving vessel. Instead, it can be pipetted into the original sample, by pressing the button to the second stop position, or released with the disposable tip, by following the step 5.

5. If the tip is to reuse for the same solution, hold the button in the first stop position for a a new aspiration and restart the procedure at step 2. If the tip is not to reuse, press the button to the second stop position over a waste vessel and then press the tip ejector button.

The immersion depth of the tip, established in the second step of both pipetting modes, can significantly affect the accuracy of the procedure and its preferable value depends on the volume to aspirate, as shown in Table 2.2. Droplets can be formed on the outside of the pipette tip if it is dipped too deeply and then they may deposit along with the liquid. In the other side, can be generated vortexing if the tip is not positioned deeply enough and, consequently, the pipette will not aspirate the intended volume of the sample [24].

Table 2.2: Optimum immersion depth according to the volume to manipulate.

Volume (µL)	Immersion Depth (mm)
0.1 - 1	1
1 - 100	2 - 3
101 - 1000	2 - 4
1001 - 10000	3 - 6

2.3.2 Robots applied to pipetting

University of Porto

The robot presented in Figure 2.4 is a system developed at the University of Porto, Portugal, which consists of a robotic arm and tool able to perform basic tasks of the pipetting technique.

The final system required the implementation of the robot UR5 from Universal Robots in order to test the gripper developed to automatize the pipetting technique. The study explored an electrical actuation approach to press the pipette buttons, through the use of a stepper motor and a servomotor. In order to allow the performance of the intended operations, a microcontroller was also used. The interaction between the robot and the laboratory operator was established by a graphic interface in web environment [22].

The tests were not possible to perform in a standard laboratory table due to the incompatibility of heights between the robot and the table, which represents a disadvantage of the work developed.

Hudson Control Group Laboratory

Two products from the Hudson Control Group Laboratory are represented in Figure 2.5, each one with different level of automation for robotic liquid dispensing.

The SOLO plus is a combination of the Hudson SOLO automatic single-channel

(a) **(b)**

Figure 2.4: Work developed at the University of Porto. In (a) is represented the robotic system for automatic pipetting and in (b) the actuation technologies used [22].

pipette and the Micro10x multi-channel dispenser. The user can accurately transfer small quantities of individual compounds and almost immediately add common solvents and reagents. This product is perfect to perform serial dilutions [26, 27].

The VaryScreen I is a multi-assay screening system that integrates plate and liquid handling robots with laboratory instrumentation. The SoftLinx software is used to control all the performed actions in a coordinated and efficient way to automate the total assay [28]. The configuration integrates the PlateCrane EX microplate robot, the dispensing module, and the multimode microplate reader with luminescence, fluorescence, and UV-Visible detectors [26].

Both systems mentioned from the Hudson Control Group Laboratory are relatively expensive, which represents a disadvantage of these products.

Andrew Alliance

Andrew, originally released in 2013, is a pipetting robot that uses conventional pipettes, non-electronic and single-channel, with a volume range from 0.1 µL to 10 mL, depending on the model selected. The compact size and the low weight allow Andrew to be easily transported and integrated into a laboratory. This robot is able to grab a pipette, insert and eject the tip, set the volume and aspirate or dispense samples with precision and high reproducibility, which increases the efficiency of a laboratory. Andrew Lab is a software platform that allows the creation and documentation of generic pipetting protocols, even without any liquid handling robot. [29, 30].

(a)

(b)

Figure 2.5: Products from Hudson Control Group Laboratory, in (a) is represented the SOLO Plus [27] and in (b) the VaryScreen I [28].

Andrew+ is the most recent liquid handling robot from Andrew Alliance and uses electronic pipettes, with a volume range from 0.2 µL to 10 mL, single and multi channel. The pipettes used are specific smart electronic pipettes from Andrew Alliance that are manufactured by Sartorius. The Andrew+ robot was designed to fit in most laboratory benches and hoods. The OneLab software allows scientists to design their own pipetting protocols in a short time [31].

Both robots from Andrew Alliance constitute expensive systems, which makes them incompatible with the economic capacities of some laboratories. Besides that, The need to invest in specific electronic pipettes represents another disadvantage of the Andrew+ robot. The Figure 2.6 shows both robots from Andrew Alliance.

(a)

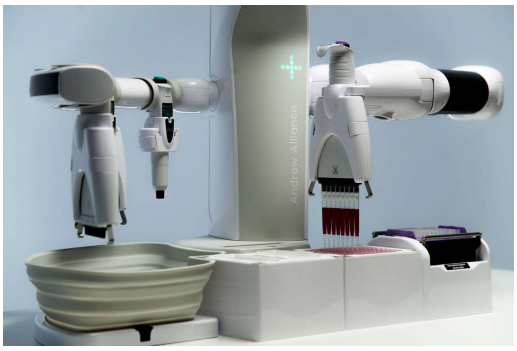

(b)

Figure 2.6: Pipetting robots from Andrew Alliance. In (a) is shown the Andrew robot [32] and in (b) is represented the Andrew+ robot [33].

Yaskawa

The MOTOMAN CSDA10F from Yaskawa is a dual arm robot designed for laboratory use without human intervention and has a maximum payload of 10 kg per arm. This robot, represented in Figure 2.7, can perform complicated automated laboratory tasks, such as sample preparation and complex workflow protocols [34].

Figure 2.7: MOTOMAN CSDA10F from Yaskawa [34].

The robot presents advantageous features like high agility and flexibility due to its 15 servo-controlled rotation axes, distributed in 7 per arm and 1 monumental axis. Besides that, this human-like system works with standard laboratory equipment, without the need to invest in expensive instruments, and allows an easy and fast programming of new tasks or work sequences [35].

Despite all the advantages mentioned, the robot from Yaskawa is an expensive system in which not all laboratories have the financial capacity to invest.

2.4 Actuation Technologies

2.4.1 Bio-inspired Actuation

Biomimetics is a relatively recent science which represents the study associated with copying, imitating, and learning from nature, by its methods, processes, and designs. This field of study is increasingly influencing new subjects, both of science and engineering, and inspiring innovative technologies [36].

Bio-inspired soft actuators are an ascending interest option due to their several applications in electronic devices, such as soft and biomedical robots, and human-friendly flexible wearable devices. Ionic soft actuators, in particular those resulting in relatively large bending mechanical deformation, are recently receiving special attention because of their biomimetic motion, small response time, flexibility, low

actuating voltage, and low cost relative to other actuation options. Besides all of the advantages, bio-inspired actuating devices, such as cellulose-based soft actuators, still present relatively low actuation performances [37].

2.4.2 Electromagnetic Actuation

A simple electromagnetic actuation solution is based on the use of a solenoid, with or without return spring. A solenoid consists of an electromechanical device that transforms electrical energy into mechanical motion, either linear or rotary. The solenoid structure includes a coil responsible for conducting current and generating a magnetic field. Solenoids also have two other required components, one to complete the magnetic circuit, which can be a case or shell of iron or steel, and one for translating motion, usually a plunger or armature. The actuation can be performed by direct or alternating current [38].

While a conventional solenoid actuator can only generate the driving force in one direction, dual solenoid actuators (DSAs) allow its generation in both directions. DSAs, represented in Figure 2.8, are based on two solenoid actuators. The lower solenoid actuator is connected to the upper one in the opposite direction in order to allow the reverse direction force generation. Basically, when the current flows in the upper solenoid actuator, is generated a magnetic force in the downward direction and when the current flows in the lower solenoid actuator, the force is generated in the upward direction. Accordingly, by changing the path of the current, a DSA generates the driving force in both directions [39].

2.4.3 Electrical Actuation

Several types of electric motors are adapted and integrated in systems of motion control due to their linear characteristics. These types include rotary and linear alternating current and direct current motors, which can be also classified into operated in closed-loop or open-loop motors. The motors usually selected for motion control systems are stepper motors and permanent-magnet direct current servomotors, either brushless or brush-type [38].

Stepper motors can be operated in an open-loop, without requiring feedback sensors, due to the control of load position and velocity by input digital pulses that are sent from the controller to the motor driver. These type of motors are reliable and economic choices for applications where low speed is acceptable and is not required the position accuracy of a servomotor [38].

Permanent-magnet direct current servomotors, either brushless or brush-type,

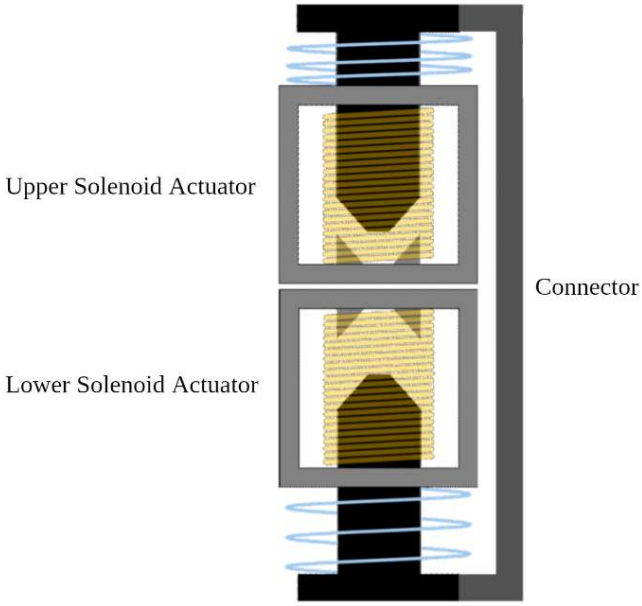

Figure 2.8: Scheme of the structure of a DSA (adapted from [39]).

are more often selected when precise positioning is required. As advantages, these motors offer higher speeds and smoother low-speed operation with a better position accuracy than stepper motors. On the opposite side, this type of motors requires feedback sensors in closed loops, which adds cost and complexity to the system [38].

The actuation speed can change under different loads, depending on the type of the selected motor. In actuators with direct current motors, speed usually changes inversely to the load, while actuators with alternating current motors operate with more constant speed. The speed can also be affected by the frequency and magnitude of the applied voltage and the environment temperature [40].

2.4.4 Pneumatic Actuation

Soft actuators are widely used to generate motion and are powered and controlled by pneumatic systems. Pneumatic supply systems are typically based on three main components, the source that generates pressurized air, valves that control flow direction, and the pneumatic line for connection [41].

The control of linear and rotary pneumatic actuators is supplied through appropriate valves, capable of controlling the air flow direction, the flow rate, and the air pressure. In most cases, the valves can be controlled through electrical signals provided by solenoids, which allows a proper interface between the microprocessor-based controller and the pneumatic actuator [42].

The pneumatic cylinder is the most recurrent type of energy transfer device

used in pneumatics and is based on a cylindrical barrel and a piston that moves in the length of the cylinder, to which a piston rod is usually attached. The linear motion of the piston is generated by applying pressurized air at one port of the ends of the cylinder [42]. The Figure 2.9 represents the mechanism of a pneumatic cylinder and its main components.

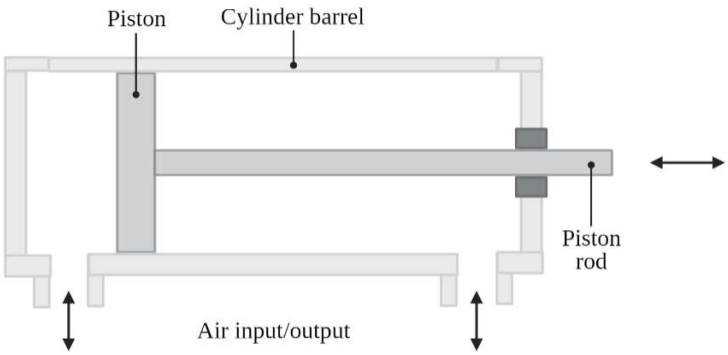

Figure 2.9: Scheme of a pneumatic cylinder (created with biorender.com).

Chapter 3

Automatizing the Pipetting Technique

This chapter describes the several studied parameters, necessary to enable the robotic system to automate the pipetting technique.

3.1 Prototype

In order to develop a system capable of automatizing the pipetting technique, it was necessary to study and implement a prototype of a robotic solution to replace the manual procedure explained in the section 2.3.1 of chapter 2.

The pipette selected for testing the automated system is a PIPETMAN Classic P100 pipette from Gilson, which is represented in Figure 3.1. This model consists on a manual air-displacement and single channel pipette with a volume range from 10 µL to 100 µL and a optimum immersion depth between 2 mm and 4 mm [43].

Figure 3.1: PIPETMAN Classic P100 pipette from Gilson (adapted from [44]).

The robotic solution developed can then be added to the cartesian robot, already in service at the Biophysics Institute of the Faculty of Medicine of the Univer-

sity of Coimbra, which was previously assembled in the Department of Mechanical Engineering of the same university. The robot integrates three linear motors, each one actuating in the perpendicular axes, X, Y and Z, and it was designed to autonomously perform CAP irradiation in cell lines [2].

Implementing a new robotic tool, the robot adopts the present function of substituting the manual performance of the pipetting technique. Therefore, depending on the specific application, it is necessary to previously study the manual procedure for designing a robotic solution that meets all the requirements.

The Figure 3.2 illustrates the movements that are supposed to be replicated by the robotic system. The first and the second ones represent the movements associated with the push button while the third one is related to the tip ejector button. All of the mechanisms are defined by linear actuation of the specific button between its initial position of resting and the final position represented in the scheme.

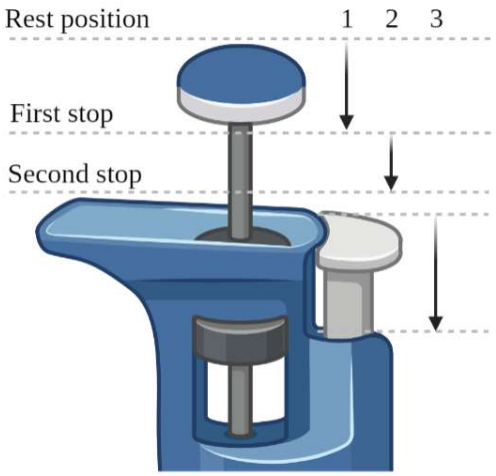

Figure 3.2: Scheme of the movements to replicate in the pipette buttons (created with biorender.com).

For automatizing the pipetting technique, it is necessary to develop an end-effector, implemented in the cartesian robot, that consists of a structure to hold the pipette in the defined position during the procedure and host the developed actuator.

To enable the activation of the buttons during pipetting operations, usually performed manually, it has to be selected an actuation mode to implement. Due to the associated requirements of this application, two approaches were considered, electrical and pneumatic actuation, following described.

3.1.1 Electrical Actuation Approach

To approach the problem with electrical actuation, it is necessary to select a motor and a control system. Three options, following described, were considered.

In the first option, a stepper motor could be used to activate the push button due to its ability to return to the original position after the complete detour. This capacity of the motor increases the accuracy and is useful in applications that prioritize precise speed, as the current movement. To perform the task associated to the tip ejector button, it could be used a servomotor, due to its high efficiency. In order to allow the performance of the previous operations, a microcontroller is required to send commands to the motor driver.

According to the requirements of the technique, a second option is possible, using servomotors to activate both of the pipette buttons. For this approach, it is necessary to implement a different structure to each motor with an appropriate format to press the specific button. The implementation of a microcontroller is also required to control the servomotors in order to execute the desired movements.

The servomotor responsible for the movements of the main button requires a maximum angle big enough to allow the associated structure to reach both stop positions of the pipette.

The servomotor responsible for the activation of the tip ejector button requires a smaller maximum angle, due to the small distance of the movement to reply, being only necessary to establish an appropriate initial position.

The structures are actuated by the servomotors with positive rotation until the angle necessary to reach a specific position and with the reverse rotation until rest position.

In order to simplify the system, a third option with only one servomotor was also considered. In this approach, it is necessary to associate a pinion and two racks to the motor. A microcontroller is also indispensable to command the servomotor to perform the required operations.

This approach also requires the implementation of a different structure to the edge of each rack. The structures must have an appropriate format in order to press the corresponding button.

3.1.2 Pneumatic Actuation Approach

Due to the requirements of this application, two pneumatic cylinders would be necessary to press the different buttons of the pipette. Besides the assembly of the pneumatic pistons, is required a connection between pipes and the cylinders with

appropriate valves and an electronic control system to control the motion of the pneumatic piston. The electronic system is responsible for manipulating the valves to release the intended air amount into the cylinder.

Accordingly, the piston is pushed in the defined direction with the appropriate force to press or release the buttons of the pipette. Therefore, double-acting pneumatic cylinders is the most advantageous option in order to allow the movement of the buttons in both directions with a controlled speed and force applied.

3.2 Requirements

The first step for developing the automated system consists of identifying significant requirements, necessary to ensure a reliable solution capable of performing the movements of the pipetting technique, previously represented in the Figure 3.2.

The requirements of the system to develop can be divided in functional and non-functional requirements. While functional requirements are associated with the system performance in a direct way, non-functional requirements are related to the environment conditions of the robotic solution.

3.2.1 Functional Requirements

To perform the pipetting technique with a conventional pipette, the automated system is required to have the ability to move the pipette buttons in the vertical axis. Therefore, the system must have only one degree of freedom (DOF).

The end-effector must allow the user to easily insert and remove the pipette and must also be adjustable to any pipette to extend this application to other options. Another requirement for the end-effector is the easy coupling to the robotic system.

The requirements for the actuation of the pipette are listed in the Table 3.1. These values were obtained with a set volume of 100 µL since it is the volume that corresponds to a higher displacement value of the push button. The values of displacement of the first and second stops of the push button correspond to the distance between the rest position of the button and its first stop and between the first and second stops, respectively. Relatively to the tip ejector button, the displacement value corresponds to the distance between its rest position and its only stop.

Table 3.1: Requirements for the actuation technology.

Parameter	Push Button First stop	Push Button Second stop	Tip Ejector Button
Force (N)	7.48	32.34	6.78
Displacement (mm)	20.2 ± 0.2	4.5 ± 0.2	8.5 ± 0.2
Dimensions (mm)	Diameter = 23.4 ± 0.2		14 ± 0.2 12.2 ± 0.2

The dimensions of the push button correspond to its diameter since it has a circular form. Regarding the tip ejector button, the dimensions represent the middle size of each side of the button since it has not a defined format. Besides these values, the distance between the opposite extreme sides of the two buttons was also measured, as represented in the Figure 3.3.

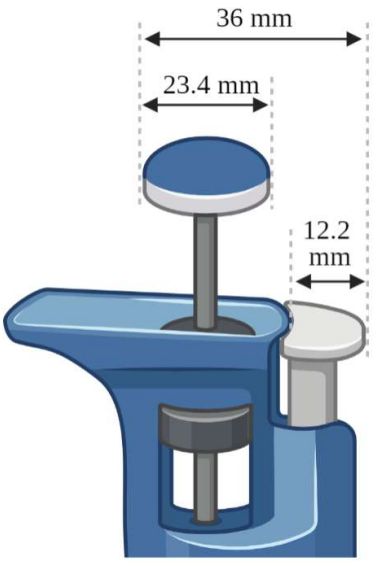

Figure 3.3: Scheme of the dimensions of the buttons and the distance between their opposite extreme sides (created with biorender.com).

According to the values measured, the maximum displacement needed to be performed by the actuator to replicate the pipetting movements is, approximately, 25 ± 0.2 mm, since the first and second stops of the push button are reached at the same axis. Furthermore, the developed system must be able to perform a maximum force of 32.34 N, approximately.

The optimum immersion depth, previously represented in Table 2.2, ranges from 1 mm to 6 mm, depending on the volume to manipulate. Since the robotic system has an accuracy of 0.004 mm in the Z axis, which is the only axis responsible

for the immersion depth of the pipette tip, the robotic system is suitable to its new application.

3.2.2 Non-functional Requirements

The system must perform the pipetting technique by aspirating a sample from a corresponding container and dispensing the solution in a wells plate. The developed solution must also be able to eject the pipette tip into a waste container after the end of the pipetting technique.

The robotic system already has a support for the well plates in its basis with the dimensions of the multiwell plate to be fixed, which are 127.76 ± 0.01 mm of length and 85.48 ± 0.01 mm of width. The area of the designed piece where the well plate is fixed has 128 mm of length and 86 mm of width [2].

To fix the sample and the waste containers, it is necessary to design and project suitable supports to implement on the table of the robotic system. With the implementation of both supports, the spatial coordinates of the containers are defined in a fixed position, allowing the robotic system to easily identify and reach them.

Accordingly, to enable the system to perform the pipetting technique, the working area of the robotic system must have space left for the supports of the sample and the waste containers.

The working area of the robotic system corresponds to the table of the cartesian robot, which dimensions are 220 mm of both length and width. Since the support of the well plate is only 128 mm of length per 86 mm of width, as already mentioned, and the dimensions of the working area of the robot are broader, remains space for the supports of the containers.

Therefore, the dimensions of the working area of the robot are adequate to meet the requirements, it is only necessary to select containers with dimensions that fit the space left and design the supports accordingly with the containers selected. Another requirement identified for the design of the supports of the containers is the easy coupling to the robot's basis.

3.3 Structural Design

According to the requirements mentioned and to the actuation approaches proposed, the solution considered the most appropriate to the problem is the electrical actuation option with one servomotor.

After the actuation mode established, it was possible to start the design process.

As an iterative procedure, several drafts were required until achieving the final structural components. All the pieces were projected in the Computer-Aided Design (CAD) software Autodesk Inventor Professional 2021.

From the requirements mentioned, it was possible to conclude that the end-effector should have an exterior structure, considered the main structure, able to couple the developed system to its destined area of the robot.

Besides, the structure responsible for the pipette support should be an individual module, specific for the pipette used, which is fixed to the main structure of the end-effector with screws. Thus, the developed system allows the future adaptation to any pipette by changing the individual module.

Therefore, it was concluded that the end-effector requires four structural components: the racks and pinion system, a top structure where the motor is fixed and the racks are supported, a bottom structure to hold the pipette, an exterior structure to join the top and bottom pieces and, finally, a coupling structure to fix the final system to its destined area of the robot.

3.3.1 Motor Selection

Since the actuator must be compact and lightweight, it is required to select a motor with these features. The servo electric motor selected to the system is the Dynamixel XL430-W250-T, which is represented in Figure 3.4 and has dimensions of 28.5x46.5x34 mm and a weight of 57.2 g.

According to the motor specifications, it achieves a maximum instantaneous and static torque of 1.4 N·m and a no load speed of 57 rpm, both at the recommended input voltage of 11.1 V. This servomotor contains a 258.5:1 gear ratio, an operating range from 0° to 360° and provides feedback of parameters that can be controlled including position, temperature, load and velocity [45].

Figure 3.4: Dynamixel XL430-W250-T (adapted from [46]).

3.3.2 Racks and Pinion System

The mechanism selected to actuate the pipette consists of a pinion, which is a toothed wheel, associated with two racks, that is, two toothed bars, each directed to one pipette button, as already mentioned.

Rack and pinion systems allow to transform the rotary motion from the selected motor into a rectilinear movement or the opposite. In this specific mechanism, by turning the toothed wheel, the teeth of the bar are driven and, consequently, the rack is moved in translation [47].

By associating two racks to the same pinion, the actuation of both buttons can be performed with only one motor, according to its rotary direction, as represented in Figure 3.5.

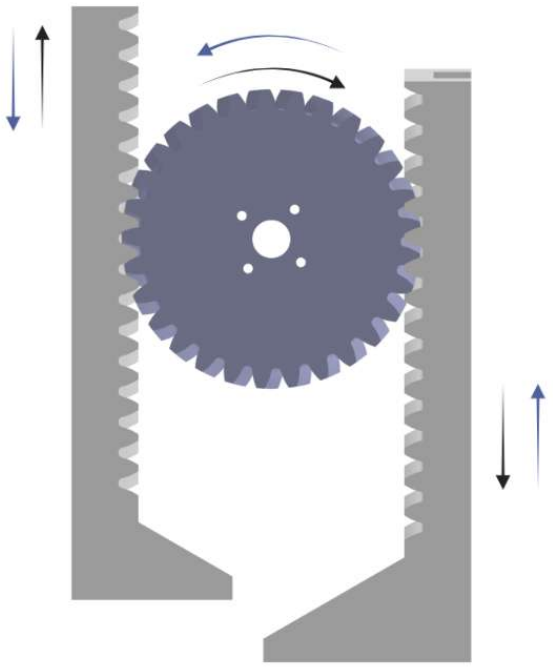

Figure 3.5: Scheme of the mechanism composed by two racks and one pinion (created with biorender.com).

The limit value for the pinion radius (r_{max}) was established by the relation between the torque of the motor (τ) and the required force to be performed (F) through the Equation 3.1. The maximum instantaneous and static torque achieved by the motor is of 1.4 N·m at the recommended input voltage (11.1 V) and the required force to execute the technique is of 32.34 N, as already mentioned. In order to prevent eventual errors in force measurement, the maximum force used in the calculations was defined as 40 N. According to the value obtained, the maximum

diameter of the pitch circle, is of 70 mm in order to perform a force of 40 N with a torque of 1.4 N·m.

$$\tau = F \cdot r_{max} \Leftrightarrow 1.4 = 40 \cdot r_{max} \Leftrightarrow r_{max} = 0.035\ m \Leftrightarrow r_{max} = 35\ mm \quad (3.1)$$

To design a gearing system, different teeth types can be considered. While in gears with straight tooth shape, the contact starts in the whole tooth width simultaneously, in gears with helical tooth shape, each tooth starts the contact at an extreme point and the contact length increases with the rotation evolution.

Therefore, in systems with helical tooth shape, the meshing between teeth occurs gradually and with less vibration, which allows prolonged teeth contact and ensures a smoother and quieter gearing operation than with systems with straight teeth [47]. Since the pipetting technique requires a smooth movement of the button, the helical tooth shape was selected for the design of the system for this application.

In Figure 3.6 is represented the pinion and rack meshing, where is visible the tangency between the pinion pitch circle and the rack pitch line.

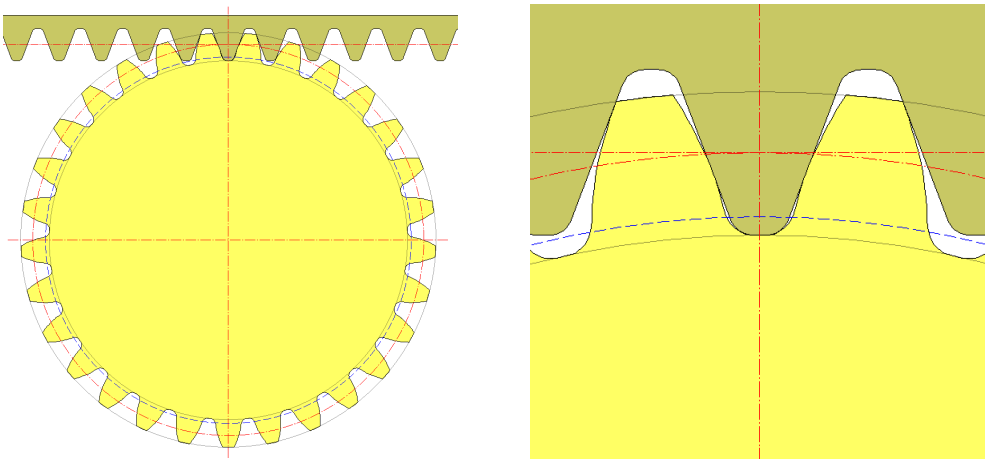

(a) **(b)**

Figure 3.6: Pinion and rack mesh. In (a) is shown a general view of the pinion and rack mesh and in (b) is represented an amplified view (adapted from Autodesk Inventor Professional 2021).

When creating a gearing system, is necessary to establish some parameters, which are following described. The pitch point is the point of tangency of the pitch circle of the pinion and the pitch line of the rack. The pitch diameter is the diameter of the pitch circle of the pinion, the module corresponds to the ratio of the pitch

diameter to the number of teeth [48].

The pressure angle corresponds to the angle between the tooth profile and the radial line at a pitch point. According to standard values, the pressure angle is 14.5° in old gears, 20° in Europe and 25° in the United States of America [47]. The helix angle corresponds to the angle between the helical tooth and the gear axis at the pitch circle and, finally, the facewidth represents the dimensional width of the gear.

The helical pinion was designed in the Autodesk Inventor Professional 2021 by exporting the tooth shape of the spur gear created with the software resource "Spur Gears Component Generator". The parameters of the spur gear used are listed in the Table 3.2.

Table 3.2: Parameters of the spur gear created with the appropriate software resource.

Module m	**Pitch Diameter** d	**Pressure Angle** α	**Helix Angle** β	**Number of Teeth** z	**Facewidth** H
2.000 mm	60.046 mm	20°	15°	29 ul	10 mm

With the tooth shape exported to a new part, the next step was to extrude the circular profile that limits the outline of the tooth shape, with the pinion thickness desired, which in this case is 10 mm.

After this extrusion, the first tooth base was created by applying the coil feature to the tooth profile through an axis of revolution with orientation equal to the helix angle. The coil behavior was defined with the method of pitch and height, where the pitch was approximately 704.014 mm, calculated through Equation 3.2, and the height was 10 mm, correspondent to the pinion thickness.

$$Pitch = \frac{d \cdot \pi}{\tan \beta} = \frac{60.046 \cdot \pi}{\tan 15} \approx 704.014\ mm \tag{3.2}$$

With the first tooth base created, the next step was to apply a circular pattern to that feature through the rotation axis of the cylinder structure, with an occurrence angle of 360° to reach the entire structure and an occurrence count of 29, equivalent to the number of teeth of the pinion. Finally, the pinion structure is finished and the last changes in its design were only due to the motor coupling, as the four holes to tighten screws. The final design of the pinion can be visualized in Figure 3.7.

The design process of the racks was similar to the pinion one. The procedure also started by exporting the tooth shape of the spur gear previously created with the software resource "Spur Gears Component Generator". The next step consisted

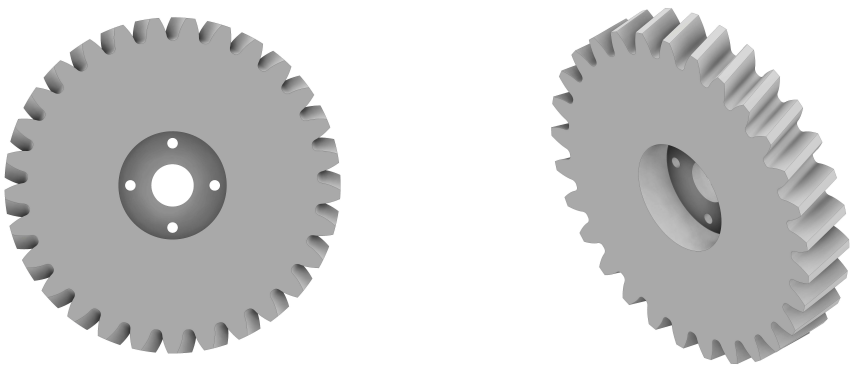

(a) **(b)**

Figure 3.7: Pinion final design. In (a) is shown the front view of the pinion draft and in (b) is represented an oblique view.

of the extrusion of a rectangular profile covering the tooth shape, with the rack thickness desired, which in this case is equal to the pinion thickness, that is, 10 mm.

With the bar created, the tool sweep was applied on the tooth profile along a path with an orientation equal to the helix angle to produce the first tooth base. With this feature created, followed the rectangular pattern to duplicate it through the bar, with a column count equal to the number of teeth of each rack and a column spacing of approximately 6.505 mm calculated through Equation 3.3. This value corresponds to the linear pitch (p) which is the linear distance between the rack teeth.

$$p = m \cdot \pi = \frac{d \cdot \pi}{z} = \frac{60.046 \cdot \pi}{29} \approx 6.505\ mm \tag{3.3}$$

By performing an extrusion in the bar, was designed an opening space on the side opposite to the teeth to allow the rack to slide through a hoist while is moved in translation.

The last changes on the design were regarding the final structure of the rack which establishes contact with the pipette buttons while pressing them. Due to the different formats and sizes of the two pipette buttons and according to the distance between the racks and the buttons in the complete system, the two racks differentiate in the final structure. In Figure 3.8 is represented the final design of one of the racks.

(a) **(b)**

Figure 3.8: Racks final design. In (a) is shown the front view of the draft of one of the racks and in (b) is represented an oblique view.

3.3.3 Parts Geometry

As already mentioned, the system requires a top structure responsible for fixing the motor and supporting the slide movement of the racks. Therefore, the final design of this structure has four holes in the lateral where will be fixed the motor. Besides, the structure was designed with an appropriate format to fit the racks. The final design of the top structure is represented in Figure 3.9, where is visible the holes to couple the motor and the hoists responsible for fit in the racks.

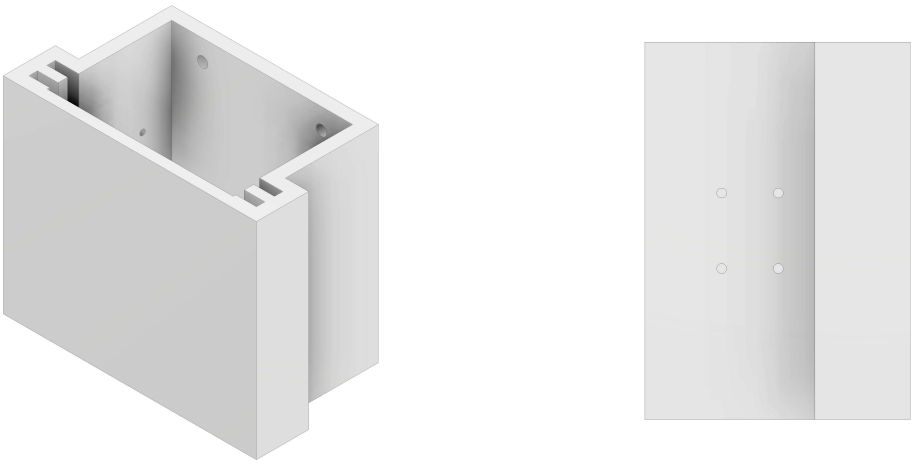

(a) **(b)**

Figure 3.9: Top structure final design. In (a) is shown an oblique view of the design of the top structure and in (b) is represented a lateral view.

Accordingly to the requirements, a bottom structure was also needed to hold the pipette. This structure, represented in Figure 3.10, presents a hole with an appropriate format to fit the pipette and a support to its finger hook. Besides, this piece has holes to fix it to the main end-effector structure and to the robot coupling

piece, following presented.

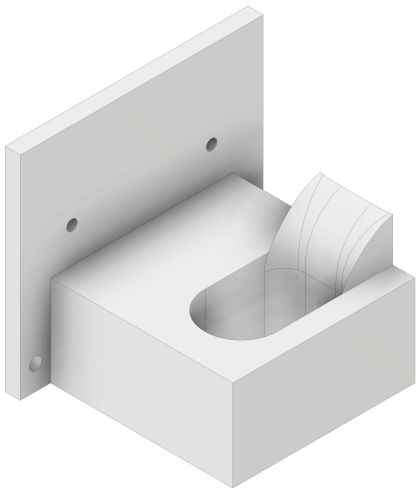

Figure 3.10: Bottom structure final design.

To fix the top and bottom pieces together, it was necessary to design an exterior structure which is represented in Figure 3.11 and has a plan geometry and holes to tighten screws.

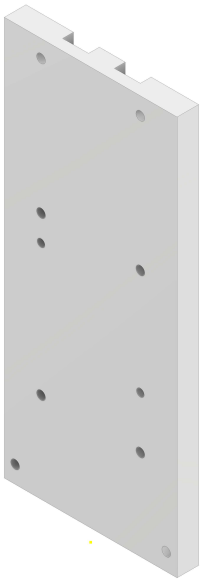

Figure 3.11: Exterior structure final design.

Finally, to couple the entire end-effector assembly to the robotic structure, it was designed a piece with an overhang that fits the end-effector area of the robot, as presented in Figure 3.12.

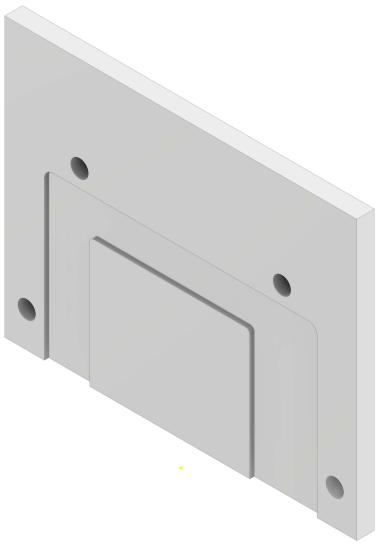

Figure 3.12: Robot coupling structure final design.

Besides the end-effector assembly itself, it was required to design a support piece to fix the two reservoirs in the table of the robotic system, one that contains the liquid to aspirate and the other to eject the tip in it. Only one design was required to print the two supports since were used two Petri dishes with the same dimensions as containers in the validation tests. The final design of the Petri dishes support is presented in Figure 3.13.

Figure 3.13: Petri dish support final design.

3.4 Structural Optimization

Several CAD software programs already offer optimization tools that can be used to improve design processes. Between those tools is the Topology Optimization from Autodesk which is an algorithmic method that predicts the performance of the design using simulation technology.

The optimization process requires a defined design with the printing material selected. If the material is not represented in the feature library, its mechanical properties can be manually inserted into the system to simulate the specific material. The next step is to apply all the forces and constraints possible to deform the piece and to establish the shape optimization criteria and mesh parameters. With all these phases completed, the simulation is ready to run.

The end-effector components that can, somehow, be affected by the tensions applied must go through validation using Finite Element Analysis (FEA) to predict possible deformations by simulating any given physical phenomenon. Since all main structures are well attached to the exterior structure, which presents a large thickness and will be printed with a high infill density, the holes where the screws will be placed to fix them do not have significant constraints. Therefore, FEA was applied only to the top structure, regarding the holes that fix the motor, to guarantee that the performance is satisfied.

To determine the force applied to the holes of the top structure that fix the motor, is necessary to understand the relation between that force and its correspondent moment. The moment of a force (M), relative to a rotation axis, is defined as the product of the force module (F) by the distance between the axis and the point of force application (d) and by the sine of the angle between the direction of the force and the referred distance (α).

Since the direction of the force applied to the holes is vertical and the distance between the hole and the rotation axis is horizontal, the angle α is 90°. Therefore, the sine is annulled and the force is calculated through Equation 3.4, being the distance between the bottom of the motor and the rotation axis of, approximately, 36 mm. According to the value obtained, the tension applied upwards to each hole is of 39 N.

$$M = d \cdot F \cdot \sin\alpha \Leftrightarrow F = \frac{M}{d} \Leftrightarrow F = \frac{1.4}{0.0036} \Leftrightarrow F = 39\ N \tag{3.4}$$

After the simulation with the obtained value for the force, the studies of the "Von Mises Stress" and the "Displacement" were considered the most significant for this analysis, whose results are represented in Figures 3.14 and 3.15, respectively.

In FEA, Von Mises stress is used to determine if a material will yield or fracture. Since the 3D printing material selected to manufacture this piece was polylactic acid

(PLA), which presents an Ultimate Tensile Strength (UTS) of 26.4 MPa, and the maximum value of the stress only reaches 0.5 MPa, the material will support the force applied.

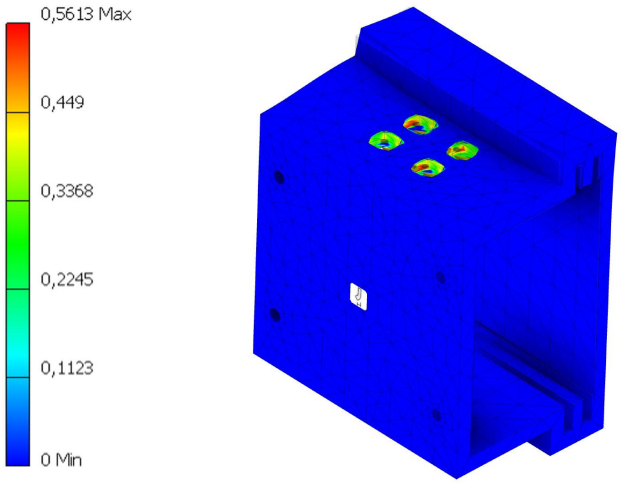

Figure 3.14: Results from the "Von Mises Stress" study with scale in MPa.

Furthermore, the displacement results allow to determining in what scale the material could deform. Since the highest value obtained for the displacement was 0.0002 mm, this parameter does not represent a constraint for the piece assembly.

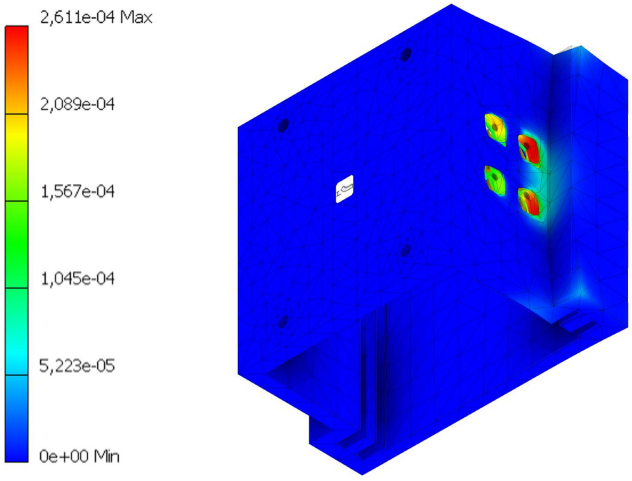

Figure 3.15: Results from the "Displacement" study with scale in mm.

3.5 End-effector Manufacturing

With the motor selected and the final geometry of the several pieces established, after the tests and necessary modifications of the initial designs, the manufacturing

process could be finally started. The end-effector development includes the 3D printing process to conceive the constituent parts and the assembly process to finish the manufacturing. For that, all the pieces were 3D printed to later perform the assembly of the end-effector.

3.5.1 Printing Process

The first step in the 3D printing process consists of saving the CAD files in Standard Tessellation Language (STL) format which describes only the surface geometry of a 3D object. This file is then introduced in a slicer software, in this case PrusaSlicer 2.3.3, to convert the 3D models into horizontal layers and trajectories that represent instructions for the printing machine to manufacture the object. With the slicing process performed, the resulting data are saved in G-code language which is compatible with the 3D printer. Therefore, the G-code file saved can be directly used in the printing machine.

The 3D printing material selected to manufacture the constituent pieces was PLA, which is a plant-based polyester. Since this thermoplastic is biologically degradable, it represents a sustainable choice for the environment. Besides, the low price and the mechanical properties following described turn the PLA the most suitable material for this application.

PLA is considered one of the materials easiest to print, allows good detail in the manufactured pieces and is not prone to warping [49]. PLA also offers a good mechanical tensile strength to the pieces, which is required in this case [50]. Although PLA presents a low resistance to temperature, tending to deform at temperatures over 60°C, it does not represent a risk in this study since the end-effector will not be exposed to those temperatures [2, 49].

Besides the material selected, the mechanical properties of the manufactured components also depend on the parameters chosen in the slicer software. The printing parameters used, which most influence the pieces properties, are reported in Table 3.3.

The 3D printer used was the Original Prusa i3 MK3S & MK3S+. This printer, when using PLA, establishes a nozzle temperature of 215°C for the first layer and 210°C for the remaining layers and the bed achieves a temperature of 60°C while printing.

Table 3.3: Printing parameters of the structural components.

	Top structure	**Bottom structure**	**Exterior structure**	**Coupling structure**	**Pinion**	**Racks**	**Petri dish supports**
Infill Density	40%	40%	50%	40%	15%	40%	5%
Infill Pattern	Gyroid	Gyroid	Gyroid	Gyroid	Gyroid	Gyroid	Gyroid
Layer height	0.15 mm	0.15 mm	0.15 mm	0.15 mm	0.15 mm	0.15 mm	0.15 mm
Type of support	None	None	None	None	None	Everywhere	None

3.5.2 Assembly Process

Since the assembly process consisted of joining all the system components, it represented a simple procedure. Firstly, the pinion was bolted to the motor and the motor fixed in the top structure through the bottom A of the motor, one of the assembly options given by the manufacturer Dynamixel [45].

The next step was to insert the racks in the right position by manually rotating the pinion to slide the bars through the top structure. With this part assembled, it was fixed to the coupling structure as well as the bottom structure. The Figure 3.16 presents the final result.

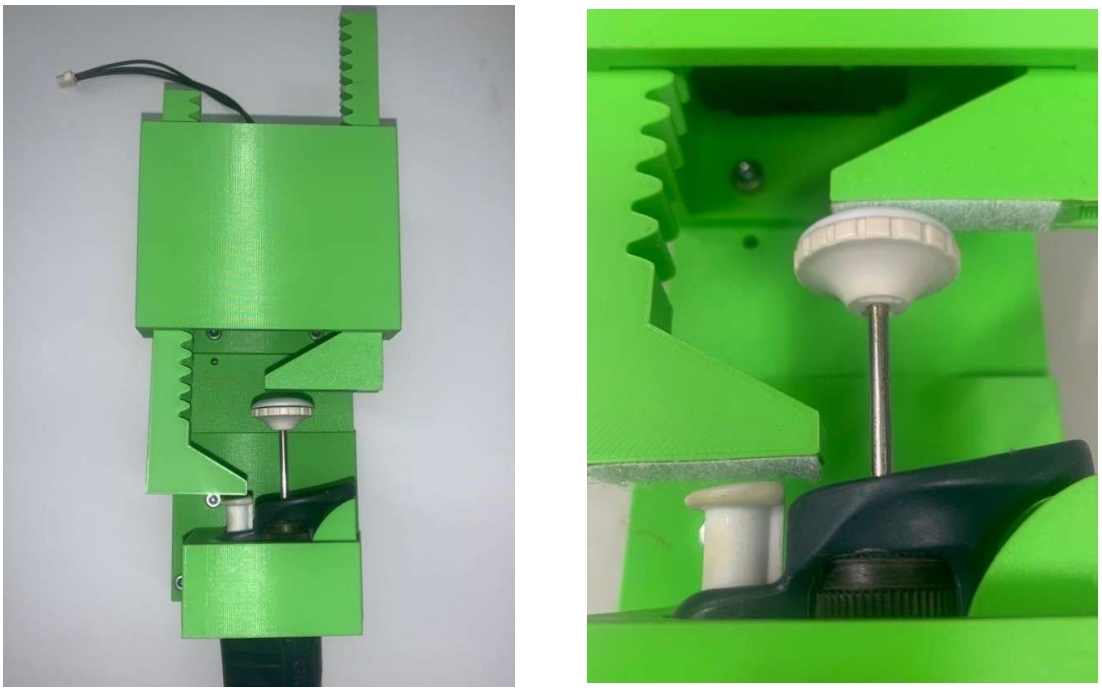

(a) **(b)**

Figure 3.16: End-effector after the assembly process. In (a) is shown a general view of the end-effector and in (b) is represented a detailed view.

3.6 End-effector Control

With the assembly process finished, followed the control of the motor in order to the end-effector perform the movements previously specified. To start the controlling process of the end-effector, the positions of the motor must be defined to the correspondent positions of the racks at the initial and final time of the movements to perform. For that, it was performed a study for the approximate angles of rotation of the motor to accomplish the required movements of the pipette buttons, following described. With those angles defined, the next step was to use DYNAMIXEL Wizard 2.0 as a tool for managing the motor from the computer to test the obtained angles, correct the eventual errors and, finally, calibrate the positions to the procedure.

3.6.1 Actuation of the Push Button

Regarding the actuation of the push button, responsible for the absorption and dispensing of solutions, the first step is to understand which volume can be manipulated. Since the pipette used has a volume range from 10 µL to 100 µL and the rest position of the push button depends on the volume to manipulate, it is necessary to establish a relation between the set volume and the rest position. The distance between the rest positions of the push button with a set volume of 10 µL and 100 µL is 18 ± 0.2 mm as represented in Figure 3.17.

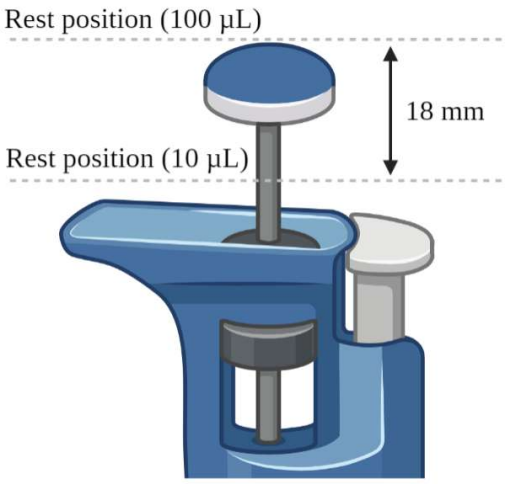

Figure 3.17: Scheme of the distance between the rest position of the push button with a set volume of 10 µL and 100 µL (created with biorender.com).

Considering the volume range, the space between the rest positions of the two limit volume values corresponds to 90 units of measurement. These obtained values

allow the calculation of the resolution by the Equation 3.5 in order to automatically define the displacement needed to be performed by the actuator to reach the positions of the push button, depending on the set volume.

$$\begin{aligned} Resolution &= \frac{Distance\ between\ rest\ positions}{Volume\ units\ of\ measurement} \\ &= \frac{18\ mm}{90\ \mu L} = 0.2\ mm/\mu L \end{aligned} \tag{3.5}$$

The only position of the push button that depends on the set volume is the rest position. Therefore, the displacement between the rest position (rp) and the first stop (fs) is always equal to the same value for a set volume of 100 µL, that is 20.2 ± 0.2 mm, less the product of the difference between the set volume and 100 µL and the resolution of 0.2 mm/µL, as represented in Equation 3.6.

$$Displacement_{rp-fs} = 20.2\ mm - ((100 - Volume)\ \mu L \times 0.2\ mm/\mu L) \tag{3.6}$$

The displacement between the first and the second stops of the push button is equal to the same value for a set volume of 100 µL, that is 4.5 ± 0.2 mm, once the position of the first stop is fixed and independent of the set volume. Therefore, to calculate the displacement between the rest position and the second stop (ss) to any set volume, is only necessary to add 4.5 mm to the obtained value of the displacement between the rest position and the first stop, as Equation 3.7 shows.

$$Displacement_{rp-ss} = (Displacement_{rp-fs}\ + 4.5)\ mm \tag{3.7}$$

As an example, if the set volume in the pipette is of 90 µL, the displacement between the rest position and the first stop of the push button would be equal to 18.2 ± 0.2 mm, as demonstrated in Equation 3.8.

$$\begin{aligned} Displacement_{rp-fs} &= 20.2\ mm\ -\ (10.0\ \mu L\ \times\ 0.2\ mm/\mu L) \\ &= (20.2\ -\ 2.0)\ mm = 18.2\ mm \end{aligned} \tag{3.8}$$

Still in the same example, the displacement between the rest stop and the

second stop of the push button would be equal to 22.7 ± 0.2 mm, which is the result of the sum of the displacement between the rest position and the first stop and the displacement between the first and second stops.

However, since the racks initial position in the movement is fixed for any set volume, the displacements between the several positions are already defined and are correspondent to the displacements to the maximum set volume, that is, 100 µL.

Since the racks are supposed to be almost in contact with the buttons in the initial moment of the movement, the displacement performed by the rack to reach the first stop is always approximately equal to 20.2 ± 0.2 mm and the displacement to reach the second stop is always approximately equal to 24.7 ± 0.2 mm, to any set volume.

Regarding the actuation of the push button of the pipette, the motor acquires negative rotation until the angle at which the rack reaches the pretended position of the button, followed by the reverse movement until the zero position.

3.6.2 Actuation of the Tip Ejector Button

Since the tip ejector button of the pipette has only one stop in a fixed position regardless of the set volume, the displacement to be performed by the system is constant for any application of the pipette. Therefore, assuming that the rack is almost in contact with the button, the rack performs a linear movement approximately equal to 8.5 ± 0.2 mm.

Regarding the actuation of the tip ejector button of the pipette, the motor acquires positive rotation until the angle at which the rack reaches the final position of the button, followed by the reverse movement until the zero position.

3.6.3 Actuator Control

After obtaining the required displacements to be performed by the system, it was necessary to calculate the estimated angles responsible for the rotational movements corresponding to the linear motions. For that, it was established that the linear distance performed by the racks is correspondent to the distance traveled by the pinion during rotational movement. Therefore, in one revolution, the linear distance is equal to the pinion circumference at the pitch diameter and is calculated through Equation 3.9.

$$Linear\ distance\ =\ \pi\ \cdot\ d\ =\ \pi\ \cdot\ 60.046\ \approx\ 188.64\ mm \tag{3.9}$$

Considering that one revolution of the pinion, that is 360° of rotation, corresponds to 188.64 mm of linear motion of the racks, it is possible to estimate the angles responsible for the required displacements of the buttons.

Attending to that, the estimated angle responsible for each displacement of the button (θ) is calculated by multiplying the correspondent displacement for the 360° of rotation, and then dividing that product for the linear distance of one revolution, that is 188.64 mm.

The estimated angles were calculated to the displacement between the rest position and the first stop of the push button by Equation 3.10, to the displacement between the rest position and the second stop of the push button by Equation 3.11 and, finally, to the displacement of the tip ejector by Equation 3.12. These values are only used for guidance when testing the motor to avoid over exceeding the supposed displacements and obtaining excessive strains.

$$\theta_{rp-fs} = \frac{Displacement_{rp-fs} \times 360^\circ}{188.64} = \frac{20.2 \times 360^\circ}{188.64} = 38.55^\circ \approx 39^\circ \tag{3.10}$$

$$\theta_{rp-ss} = \frac{Displacement_{rp-ss} \times 360^\circ}{188.64} = \frac{24.7 \times 360^\circ}{188.64} = 47.14^\circ \approx 47^\circ \tag{3.11}$$

$$\theta_{tip\ ejector} = \frac{Displacement_{tip\ ejector} \times 360^\circ}{188.64} = \frac{8.5 \times 360^\circ}{188.64} = 16.22^\circ \approx 16^\circ \tag{3.12}$$

With these approximate angles defined, the tool Dynamixel Wizard 2.0 was used for managing the motor from the computer to test the obtained angles, correct the errors and, finally, calibrate the positions to the procedure, as already mentioned. The first step was to adjust the initial position of the racks as close as possible to the buttons, by setting the correct rotation angle of the motor for that. This rotation angle of the motor in the initial moment corresponds to the zero position and was defined as 72.60°.

Then, regarding the actuation of the push button of the pipette, the initial angle of the motor was decreased by the the values obtained in Equations 3.10 and 3.11 to test those displacements, since the motor acquires negative rotation to

slide down the correspondent rack. Relatively to the actuation of the tip ejector button of the pipette, since the motor acquires positive rotation to slide down the correspondent rack, the initial angle of the motor was increased by the the value obtained in Equation 3.12.

After these tests, it was possible to set the correct position angles of the motor to perform each movement of the pipette buttons. The obtained values are presented in Table 3.4.

Table 3.4: Correct position angles of the motor to perform the movements of the pipette buttons.

Movement	**Zero Position**	**Push Button First Stop**	**Push Button Second Stop**	**Tip Ejector Button**
Goal Position	72.60°	26.37°	8.79°	96.68°
Real Position	72.60°	29.53°	20.65°	92.46°

Since there is a distance between the bottom of the racks and the surface of the buttons that was not considered in Equations 3.10, 3.11 and 3.12, the set angles are not equal to the supposed ones accordingly to the values obtained in those calculations. Besides, the acquired position and the goal position showed a variation during the procedure, which also contributes to this difference between the calculated and the defined angles. Therefore, to reach a specific position of the rack, it was necessary to increase the difference angle between the zero position and the goal position of the motor.

With the correct angles defined, it was finally possible to control the motor using the microcontroller Arduino Uno combined with the Dynamixel shield board from Robotis. The software used to control the Arduino board was the Arduino Integrated Development Environment (IDE) in the version 1.8.16. The first step was to ensure that the software connects to the correct Arduino board by defining the corresponding serial port.

Firstly, to only test the motor control, the Arduino Uno was powered by the computer and the Dynamixel shield board by an external power supply. To program the Dynamixel shield via Arduino IDE, two libraries were needed, "Dynamixel2Arduino" and "Dynamixel Shield". With this setup was possible to control the motor to reach the required positions.

To execute this specific application, one program was created, with three differ-

ent commands, each to perform one of the movements of the pipette buttons, that is, one until the zero position of the motor which corresponds to not pressing any button, one until the position correspondent to the first stop of the push button and the last one relative to the tip ejector button.

With the motor control via Arduino projected, the next step was to establish the connection between the robot and the Arduino. The commands for the motor control are triggered by the reception of a signal from the robotic system, through a digital input on the Arduino. Initially, the idea was for both the Arduino Uno and the Dynamixel shield board to be powered by the robot. However, since the signal transmitted by the robot had associated noise that was compromising the reception of the signal responsible for the motor commands, it was chosen to supply power to the Arduino and Dynamixel boards from external sources. The communication between the Arduino Uno, the Dynamixel shield board, the motor and the robot is schematized in Figure 3.18.

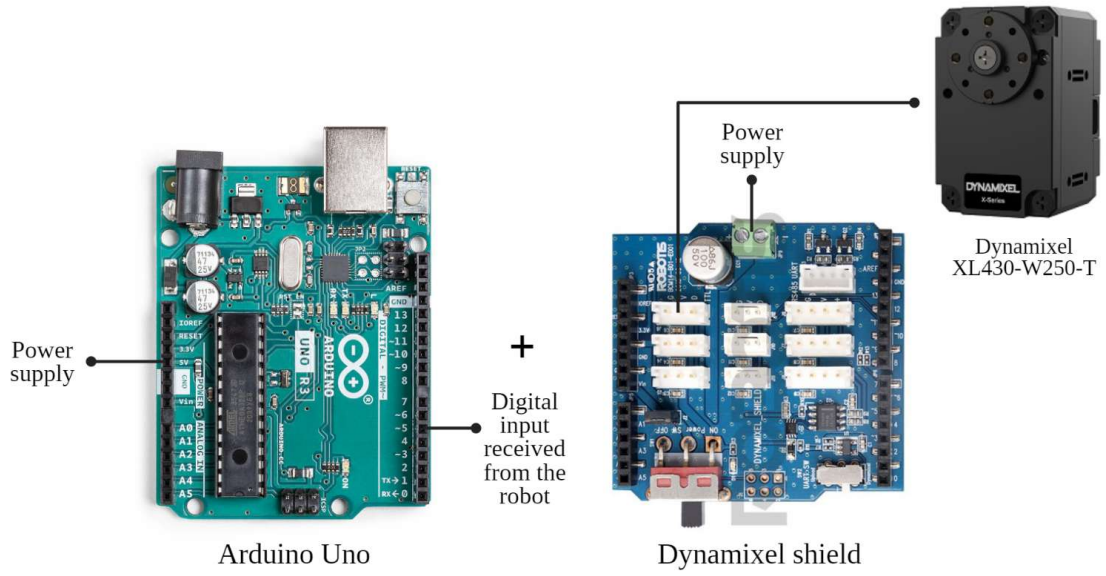

Figure 3.18: Scheme of the communication between the Arduino Uno, the Dynamixel shield board, the motor and the robot (created with biorender.com and components images adapted from [46, 51, 52]).

Depending on the duration of the received signal, each one of the three different commands is activated. For that, the signal duration must be defined in the corresponding parts of the G-code, which is later processed by the robotic system to perform the pipetting technique.

In the language G-code, the commands used to activate and inactivate the signal were the codes “M106” and “M107”, respectively. Between these two lines, the G-

code file must have the code "G04 P", followed by the required time in milliseconds, for pausing the program. In the Arduino program, it was defined that if the signal duration was between 500 and 699 milliseconds the mechanism will reach the rest position, between 700 and 899 milliseconds the first stop of the push button is reached and between 900 and 1099 milliseconds the tip ejector button will be pressed.

With the system finally assembled, the Arduino Uno and the Dynamixel shield board were fixed to the lateral of the robot structure and the end-effector was coupled to its destined area. The final robotic system is presented in Figure 3.19.

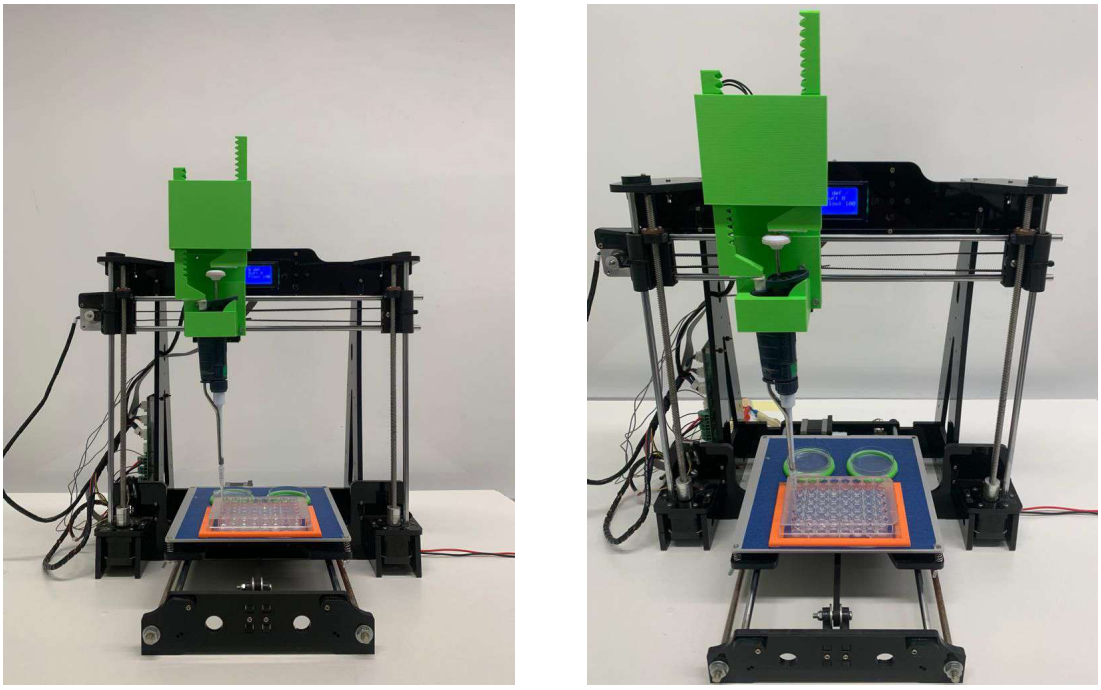

(a) **(b)**

Figure 3.19: Final robotic system.

Chapter 4

Application of Cold Atmospheric Plasma in Microorganisms

This chapter describes the procedures performed in order to study the effects of the application of Cold Atmospheric Plasma (CAP) in bacteria, filamentous fungi and yeasts.

4.1 Robotic System Programming

For this application, the robotic system is controlled using the programming language G-code, which contains commands for the linear movements to be performed by the end-effector. This type of language allows to program and control the linear motors of the robotic system with a compact and intuitive code.

To program the robotic system in order to execute the required procedures, it was necessary to manually determine the spatial coordinates in the robot table of the wells of a 48-well plate, the type of well plate where the CAP irradiation would be later performed.

The wells of a 48-well plate are positioned in a matrix 6x8 with lines denominated by the letters from A to F starting at the top and columns identified by the numbers from 1 to 8 starting on the left. The identification of the wells is schematized in Figure 4.1.

With the coordinates of the wells defined, it was possible to write a G-code responsible to perform the procedure. The file was later saved in the SD card and introduced in the robotic system.

The coordinates of the positions are defined relatively to the origin which is located in the top left corner of the table of the robotic system. These spatial coordinates are presented in units of millimeters.

In G-code, the command "G28" is used to return the end-effector to its zero

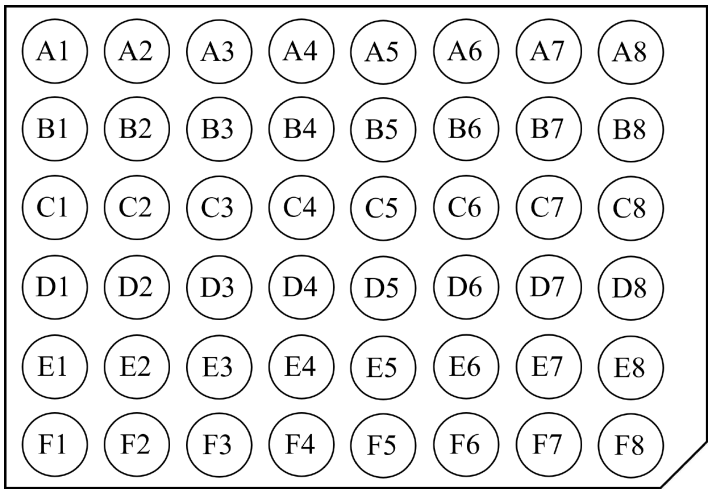

Figure 4.1: Identification of the wells of a 48-well plate.

position, which, in this system, corresponds to the point of coordinates (-50,10,0) mm. The command "G0" is responsible for linear movements and the spatial coordinates presented after the code represent the position of the end-effector in the final of the movement.

The irradiation time is defined to each well by using the code "G04" followed by P command with the time that the end-effector is positioned in the well, in milliseconds.

As an example, the following G-code corresponds to the movement of the end-effector to the position of the well F1 of the 48-well plate for 30 seconds.

```
G28
G0 Z50
G0 X30 Y126 Z50
G0 Z30
G04 P30000
G0 Z50
G28
```

The first and last lines command the end-effector to return to its zero position. The second, fourth and sixth lines command the end-effector to reach the Z coordinate at the introduced value keeping the remaining coordinates. The third line is responsible to move the end-effector to the spatial coordinates inserted and the fifth line presents the code to pause the program during 30 seconds.

4.2 Microorganism Cultures

The procedures of cultures manipulation were performed by the Medical Microbiology Group of the Centre for Neuroscience and Cell Biology (CNC) at the Faculty of Medicine of the University of Coimbra (FMUC), Portugal. Between the microorganisms irradiated were 2 cultures of yeasts, 4 types of filamentous fungi and 3 bacterial strains, a total of 9 well plates, one for each microorganism.

4.2.1 Bacterial Strains

The antibacterial assays were performed against one gram-positive bacteria: *Staphylococcus aureus* and two gram-negative bacteria: *Escherichia coli* and *Pseudomonas aeruginosa* obtained from the collection of Institute of Microbiology, FMUC.

The assay was done according to standard M07-A10 of the Clinical Laboratory Standards Institute. Briefly, overnight cultures of each strain were transferred into a tube containing 2 mL of normal saline (NaCl 0.9%), until the turbidity standard of 0.5 McFarland.

A 48-well microtiter plate was inoculated with 500 µL of Muller-Hinton broth medium and 50 µL of the bacterial suspensions in a final concentration of 5x104 Colony Forming Unit (CFU)/well. In the assay was included a bacterial growth control in Muller-Hinton medium without irradiation to assess the viability of each bacteria tested and a sterility control of the culture medium, Muller-Hinton without inoculum.

4.2.2 Fungal Strains

The fungal strains *Candida albicans* YP0037, *Candida parapsilosis* YP0515, *Trichophyton rubrum* IMF028, *Trichophyton mentagrophytes* IMF029, *Alternaria alternata* IMF030 were obtained from the Microbiology Pathogenic Yeast Collection of the University of Coimbra.*Aspergillus fumigatus* CBS 500.90 was obtained from CBS-KNAW Fungal Biodiversity Centre (Utrecht, The Netherlands).

Yeast strains were grown on Yeast Extract Peptone Dextrose (YPD) agar plates with the following composition: 0.5% yeast extract (Panreac), 1% peptone (Panreac), 2% agar (Cultimed) and 2% glucose (Sigma-Aldrich) (w/v). Yeasts were inoculated and incubated at 30ºC.

Filamentous fungi strains were grown on Potato Dextrose Agar (Difco). *T. rubrum*, *T. mentagrophytes*, *A. fumigatus* were inoculated and incubated at 30ºC. *A. alternata* were inoculated and incubated at 30ºC with alternating 16-h light 8-h

dark cycle under a BLB blacklight blue lamp (15 W).

The inoculum was prepared following the standardized protocol M27-A2 method for yeasts and the M38-A2 protocol for filamentous fungi developed by the Clinical & Laboratory Standards Institute (CLSI) to determine the Minimum Inhibitory Concentration (MIC) of antifungal compounds.

The yeast inoculum was prepared by picking three 24-h-old colonies of *Candida* spp. The colonies were suspended in sterile 0.85% saline solution and the cell density was adjusted to match an optical density (OD_{530nm}) of 0.5 McFarland at 530 nm. The suspension was made by a 1:100 dilution with sterile 0.85% saline solution followed by a 1:20 dilution with RPMI 1640 broth medium.

For the dermatophytes inoculum preparation, mycelia of *Trichophyton* spp. with 5-7 days were covered with 1 mL of sterile 0.85% saline and a suspension was prepared by gently probing the colonies with a sterile swab. The suspension resulted in a mixture of spores and hyphal fragments that was left to settle for five minutes. The conidia were counted in a hemacytometer and the concentration was adjusted by diluting the suspension with RPMI 1640 to a final concentration of 2000-6000 CFU/mL.

For *A. fumigatus* inoculum preparation, were used mycelia with 48 hours. These were covered with 1 mL of sterile 0.85% saline and one drop of Tween 20. The suspension resulted in a mixture of spores and hyphal fragments that was left to settle for five minutes. The OD_{530nm} was read and adjusted to 0.09-0.13. The suspension was diluted 1:50 with RPMI 1640.

For *A. alternata* inoculum preparation, were used mycelia with 2 weeks. Mycelia were covered with 1 mL of sterile 0.85% saline and a suspension were prepared by gently probing the colonies with a loop. The suspension resulted in a mixture of spores and hyphal fragments that settled for five minutes. The OD_{530nm} was read and adjusted to 0.25-0.30. The suspension was diluted 1:20 with RPMI 1640.

500 µL of each inoculum were loaded in a 48 wells flat-bottom plate (triplicates for each time of irradiation tested).

Each assay included triplicates of growth control of the inoculum (in RPMI-1640 medium) without irradiation to assess the viability of each organism tested and a sterility control consisting in RPMI-1640, without inoculum.

4.3 Cold Atmospheric Plasma Irradiation

As already mentioned, the end-effector holds the needles connected to crocodile electric plugs, correspondent to the electrodes responsible for plasma and current

conduction from the device. Since the CAP discharge implies a close approximation of the electrodes to the sample, the needles were changed between the application of CAP in different cultures in order to avoid contaminations of the samples. The Figure 4.2 represents the robotic system performing the application of CAP.

The CAP irradiation was performed by the robotic system in 48-well plates. Three lines (from A to C) and five columns (from 1 to 5) of each well plate were used in the tests. As already mentioned, the first column was filled with a sterility control in order to allow the detection of contaminations and the second column had the growth control of the inoculum to compare with the cultures irradiated with CAP.

The last three columns had the cultures in which the CAP was applied, being the third column irradiated during 30 seconds, the fourth during 60 seconds, and the last one during 120 seconds. Each well was filled with 500 µL of the inoculum in order to avoid significant differences in the position of the needles relative to the solution between wells.

Before the CAP application in the microorganisms, the setup was performed in the well F1 which was filled with 500 µL of water in order to calibrate the position of the needles for the procedure.

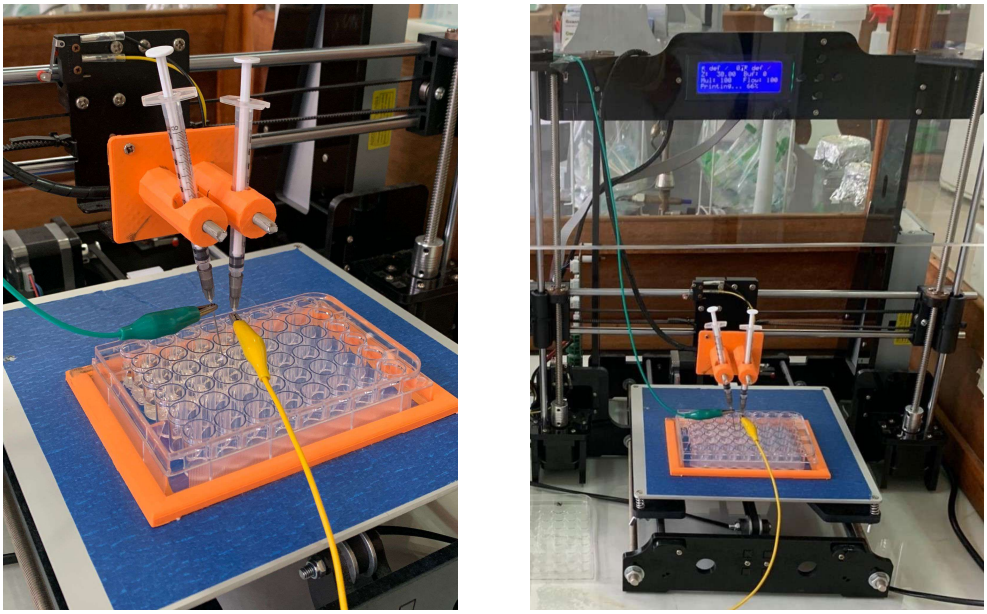

(a) **(b)**

Figure 4.2: The robotic system performing the application of CAP.

4.4 Viability Tests

After irradiation for 30 seconds, 1 minute and 2 minutes the plates with the bacterial strains were incubated at 37ºC for 24h and the bacterial growth was determined by absorbance at 600 nm using a microplate reader (SpectraMax® Plus384, Marshall Scientific, Hampton, EUA), comparing growth between bacterial growth control and bacterial suspensions subject to irradiation treatment. The MIC is defined as the lowest concentration at which the microorganisms do not demonstrate visible growth. All the determinations were done in triplicate.

The bacterial suspensions from the wells which did not show any growth after incubation during MIC assays were plated on Columbia agar medium followed by counting the CFU after 18-24h of incubation at 37ºC to determine the reduction in bacterial population induced by the irradiation treatment.

The count of CFU is performed through a serial dilution of the original sample in order to achieve a sample with a countable number of colonies. In Figure 4.3 is represented the process of the determination of CFU/mL, which is calculated through the Equation 4.1.

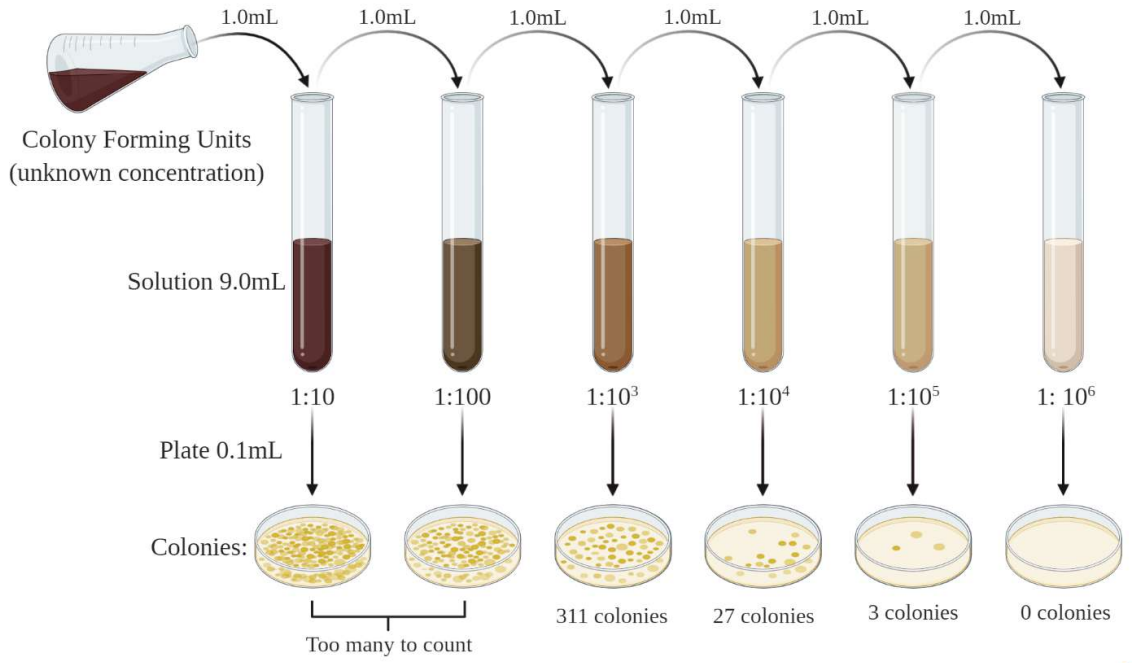

Figure 4.3: Scheme of the determination of CFU/mL through serial dilution. (created with biorender.com).

$$CFU/mL = \frac{Number\ of\ colonies\ on\ plate \times Dilution\ factor}{Volume\ of\ culture\ plate\ (mL)} \tag{4.1}$$

In the case of the example on Figure 4.3, supposing that the plate of the 10^3 dilution yielded a count of 311 colonies, the number of bacteria per mL of the original sample is given by Equation 4.2.

$$CFU/mL = \frac{311 \times 10^3}{1} = 3.11 \times 10^5 \ CFU/mL \tag{4.2}$$

Regarding the fungal strains, after exposure to irradiation, the plates were incubated at 37ºC, for 48h for *Candida* spp., 72h for *A. alternata* and 96h for *Trichophyton* spp. and *A. fumigatus*, as recommended by the standards. The reading of the plates with the fungal strains was done visually, comparing growth between control and radiation exposure times.

Chapter 5

Results and Discussion

This chapter presents the analysis of the validation tests of the developed end-effector and the discussion of the results from the application of Cold Atmospheric Plasma (CAP) in microorganisms.

5.1 Validation Tests of the Pipetting Technique

To validate the developed system and to evaluate its influence in laboratory time management, were performed experimental tests and the results between the manual and the automated pipetting were compared.

5.1.1 Robotic System Programming

As already mentioned in chapter 4, the robotic system is controlled using the programming language G-code, which allows to program and control the linear motors to perform the required movements of the end-effector. Since the robot will not be only used for executing the pipetting technique, the end-effector is changed according to the laboratory task to be performed next. For other applications than pipetting, the G-code files frequently start and end with the "G28" code that commands the end-effector to return to its zero position, which in this system, corresponds to the point of coordinates (-50,10,0) mm, as already mentioned.

Nonetheless, the high dimensions of the end-effector that performs the pipetting technique disable the use of the command "G28" while the end-effector is fixed in its destined area of the robot. Therefore, the pipetting technique must always start and finish with a specific value for the Z axis, corresponding to the height of the end-effector that does not cause any damage.

However, when the robot initiates with the axes out of the zero position, it assumes the values of each axis as 0 mm. To avoid this issue, the solution considered the most appropriate is based on two additional steps, besides the pipetting

technique itself, following described.

The first step consists of creating a G-code file to execute the setup of the end-effector, which only moves the Z axis to an appropriate height to later couple the end-effector. After fixing the end-effector to its destined area of the robot, the main G-code is executed to perform the pipetting technique. The last step corresponds to returning all axes to the zero position after finishing the pipetting technique and before turning off the robot. To execute this step, is only necessary to select the option "Home All" in the "Quick Settings" of the robot main menu.

The only possible disadvantage of this solution is the time spent inserting and removing the end-effector. However, since the system of coupling the end-effector to the robotic system is of easy handling this does not represent a problem.

The pipette used in the tests was a PIPETMAN Classic P100 pipette from Gilson, which is a manual air-displacement and single channel pipette with a volume range from 10 µL to 100 µL. Besides, this model has an optimum immersion depth of the tip between 2 mm and 4 mm, and was performed the forward mode pipetting in the assays.

To validate the robotic system for the pipetting technique, it was defined that the end-effector would aspirate the liquid from a Petri dish, dispense the liquid in the wells of a 48-well plate and eject the tip into a different Petri dish. The scheme of the 48-well plate is presented in Figure 4.1 of chapter 4.

With the programming option selected, the first step was to manually determine the spatial coordinates in the robot table of the wells of a 48-well plate and of the two Petri dishes used. For that, their supports were fixed on the robot basis and the end-effector was moved through the robot commands within the option "Position" of the main menu.

Once the pipette is properly positioned, the values of the three axes are annotated. The positions of the X and Y axes were taken when the pipette tip was framed at the middle of the wells or the Petri dishes. Four values were obtained for the Z axis, following described. One value refers to when the pipette tip is above the dishes and the well plate to allow the free movement of the end-effector. The second position of the Z axis is to insert the pipette tip into the liquid to aspirate it with approximately 3 mm, since the optimum immersion depth of this pipette is between 2 mm and 4 mm. The third value corresponds to the height of the end-effector in the moment of dispersion of the liquid in the well. Finally, the last one allows the ejection of the pipette tip into the correspondent Petri dish.

5.1.2 Validation of the Pipetting System

The first step to validate the entire system consisted of testing the end-effector before associating it to the robot. For that, were performed validation tests of the pipetting technique executed both manually and automatized. These validation tests were based on weighing the liquid pipetted and comparing the obtained measures to the set volume on the pipette.

The pipetting technique was performed 10 times to a container, which was initially weighted while empty. After the manipulation of the intended volume to the well, which in this case was 100 µL, the container was weighed again for each manipulation. The difference of weights corresponds to the weight of the volume pipetted. The mass was measured with a ES-3000A scale from Techmaster, which has an uncertainty of 0.1 g.

Since the tests were performed using water as the liquid manipulated, which specific mass is approximately 1 g/cm^3, the resulting difference of mass was converted to the corresponding volume quantity in µL through Equation 5.1.

$$\rho\ (g/cm^3) = \frac{m\ (g)}{V\ (cm^3)} \Leftrightarrow V\ (cm^3) = \frac{m\ (g)}{\rho\ (g/cm^3)} \Leftrightarrow V\ (\mu L) = \frac{m\ (g) \times 10^3}{\rho\ (g/cm^3)} \quad (5.1)$$

The results of the automatized pipetting performed by the end-effector showed that the difference of the container weight before and after the pipetting, was correct to all assays since it was always equal to 0.1 g which corresponds to 100 µL. However, the scale has an uncertainty of 0.1 g, which does not allow conclusions about the accuracy of the manipulated volume. Lastly, the entire robotic system was tested regarding the spatial coordinates measured. These tests showed that the robot achieves with precision each required position.

The pipetting technique performed manually represents a highly time-consuming task in laboratory, since it is a common task executed several times a day, as already mentioned. Besides, the time spent by the laboratory operator on this repetitive technique, could be used instead in high value-added tasks. During the manual performance of the technique, the researcher is highly focused on the procedure, whereas with the automatized pipetting the researcher could be focused on other useful tasks at the same time since is not necessary to interact with the system.

5.2 Results and Discussion of CAP Irradiation

This section presents the results obtained with the application of CAP in microorganisms and the discussion of the potential of CAP irradiation as an antimicrobial treatment to the microorganisms tested.

5.2.1 Bacterial Strains

After the application of CAP, the bacterial growth was determined by absorbance at 600 nm using a microplate reader after the incubation of the plates. Besides, was performed the Colony Forming Unit (CFU) counting of the bacterial suspensions from the wells which did not show any growth during Minimum Inhibitory Concentration (MIC) assays. The results of the reduction in bacterial population induced by the CAP irradiation treatment are following presented to each bacteria.

Escherichia coli

Relatively to the gram-negative bacteria *Escherichia coli*, the CAP irradiation treatment of 2 minutes showed a reduction of approximately 99% of the initial population, while the exposure of 30 seconds and 1 minute presented no effect. These results can be interpreted in Figure 5.1 through the turbidity visualized in the columns of the well plate, which represents the bacteria growth of the population.

While the turbidity is high and practically equal in the second, third and fourth columns, correspondent to the growth control of the inoculum and to the exposure times of 30 seconds and 1 minute, respectively, the last column shows significantly lower turbidity, barely noticeable. Furthermore, it is also visible some turbidity in the third line of the first column which suggests a contamination of the sterility control, probably due to the proximity of the cables of the CAP discharge machine to the plate.

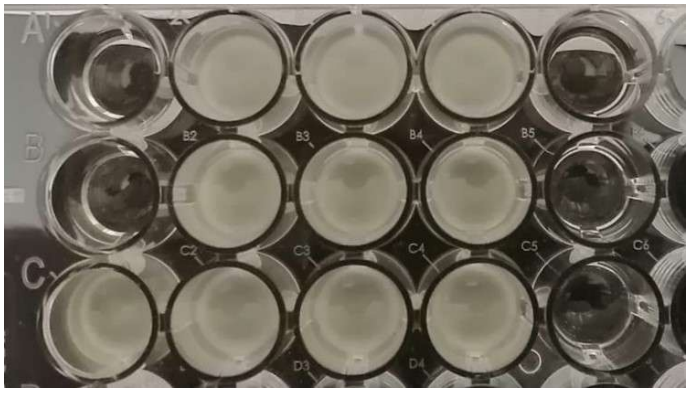

Figure 5.1: 48-well plate containing *Escherichia coli* after CAP irradiation.

Pseudomonas aeruginosa

Regarding the gram-negative bacteria *Pseudomonas aeruginosa*, the CAP irradiation with exposure times of 60 seconds and 120 seconds showed a bactericidal effect and the treatment with only 30 seconds already showed a reduction of approximately 90% of the initial population. These results can also be interpreted in the Figure 5.2 also through the turbidity visualized in the different columns of the plate.

While in the second column, correspondent to the growth control of the inoculum, is visible a high turbidity resultant of the bacteria growth, in the third column, which was irradiated for 30 seconds, the turbidity of the medium appears to be significantly lower. Furthermore, the last two columns, which were exposed to CAP for 1 and 2 minutes, appear to show no turbidity.

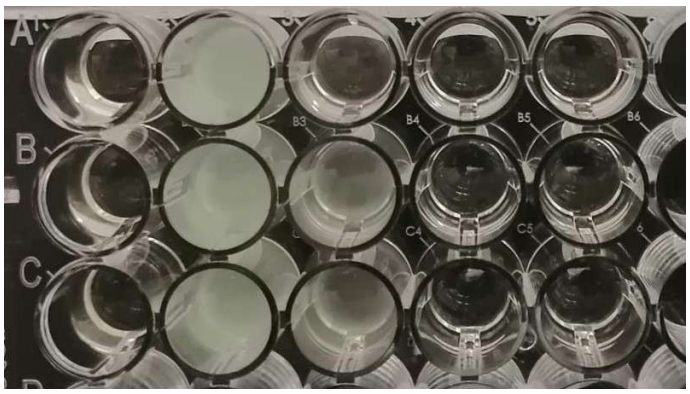

Figure 5.2: 48-well plate containing *Pseudomonas aeruginosa* after CAP irradiation.

Staphylococcus aureus

The antibacterial assays performed against the gram-positive bacteria *Staphylococcus aureus* showed a bactericidal effect for the treatment with exposure for 2 minutes and no effect to the irradiation times of 30 seconds and 1 minute. These results are visible in Figure 5.3 through the turbidity visualized at the different columns.

The turbidity is practically equal at the second, third and fourth columns, corresponding to the growth control of the inoculum and the wells exposed to CAP irradiation for 30 seconds and 1 minute, respectively. However, some wells of the last column show significantly lower turbidity, barely noticeable, corresponding to no growth of the population. The turbidity visible at the well of the first line and the third column might be a result of a variation on the current of the CAP discharge machine during the exposure.

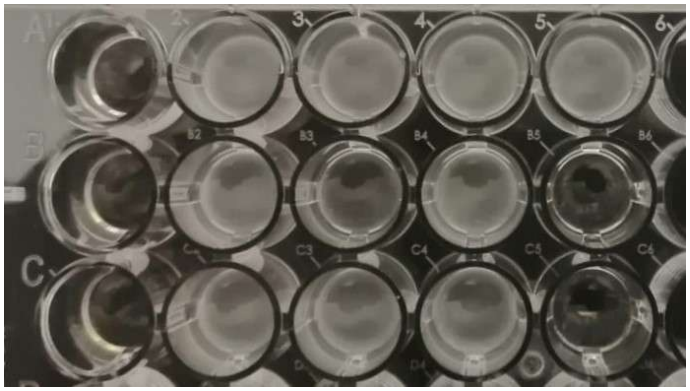

Figure 5.3: 48-well plate containing *Staphylococcus aureus* after CAP irradiation.

5.2.2 Fungal Strains

After the exposure to CAP irradiation, the fungal strains were analysed after the incubation of the plates and the reading of the growth was done visually. The conclusions of the reduction in fungal population obtained with the visualization of the well plates are following described to each strain.

Candida albicans* and *Candida parapsilosis

Comparing the visual reading of the plates containing the yeasts *Candida albicans* and *Candida parapsilosis*, it is concluded that both strains show the same results. In Figure 5.4 it is possible to detect the colonies, which seem to be practically equal between the control and the three exposed columns. Therefore, there

is no growth inhibition resultant of the CAP irradiation at least with the exposure times tested.

Furthermore, it is detected a color change that increases with the exposure time. Since this color change was not observed in the bacteria assays and was not immediate, it may be caused by a change in one of the constituents of the culture medium or by a metabolic alteration of the microorganism that led to a pigment production.

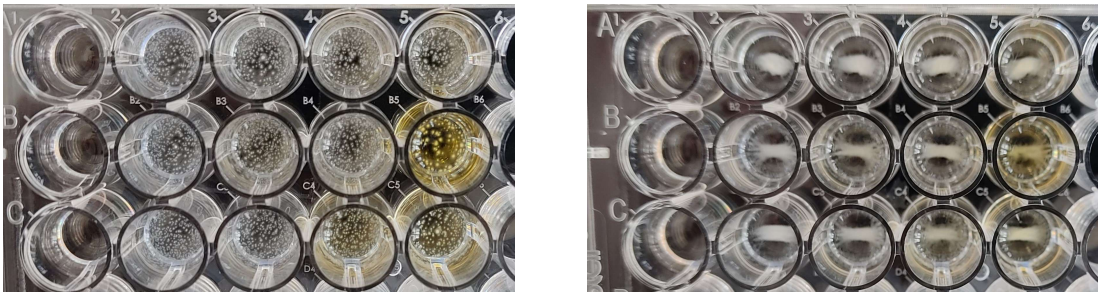

(a) **(b)**

Figure 5.4: 48-well plates containing *Candida* spp. after CAP irradiation. In (a) is shown the well plate containing *Candida albicans* and in (b) is the well plate containing *Candida parapsilosis*.

Trichophyton rubrum and *Trichophyton mentagrophytes*

Plates containing *Trichophyton rubrum* and *Trichophyton mentagrophytes* showed the same results in the visual reading. In Figure 5.5 it is possible to detect small colonies at the bottom of the well, which seem to decrease with the exposure time. However, growth inhibition is only clear at the column with 2 minutes of exposure. Therefore, the fungicidal effect is probably only reached after 2 minutes of CAP irradiation.

Furthermore, a color change is also detected in the culture medium although not as evident as in other microorganisms. As already mentioned, this change may be caused by a modification in a constituent of the culture medium or by a metabolic alteration of the microorganism.

Aspergillus fumigatus and *Alternaria alternata*

The visual reading of the plates containing *Aspergillus fumigatus* and *Alternaria alternata* presented a growth inhibition at all columns exposed to CAP when compared to the growth control, but the inhibition was only significant at the wells irradiated for 2 minutes. These results can be interpreted in Figure 5.6 through the

(a) **(b)**

Figure 5.5: 48-well plates containing *Trichophyton* spp. after CAP irradiation. In (a) is shown the well plate containing *Trichophyton rubrum* and in (b) is the well plate containing *Trichophyton mentagrophytes*.

turbidity visualized at the wells, as in the case of bacteria.

Despite being more visible in the plates containing *Aspergillus fumigatus*, the turbidity clearly decreases with the exposure time in both fungal strains. The turbidity decrease translates into a higher growth inhibition and the last column shows barely noticeable turbidity, corresponding to almost no growth of the population.

Besides, an evident color change is detected in the culture medium of *Aspergillus fumigatus*, which increases with the exposure time and may be caused by a modification in a constituent of the culture medium or by a metabolic alteration of the fungal strain that led to the pigment production.

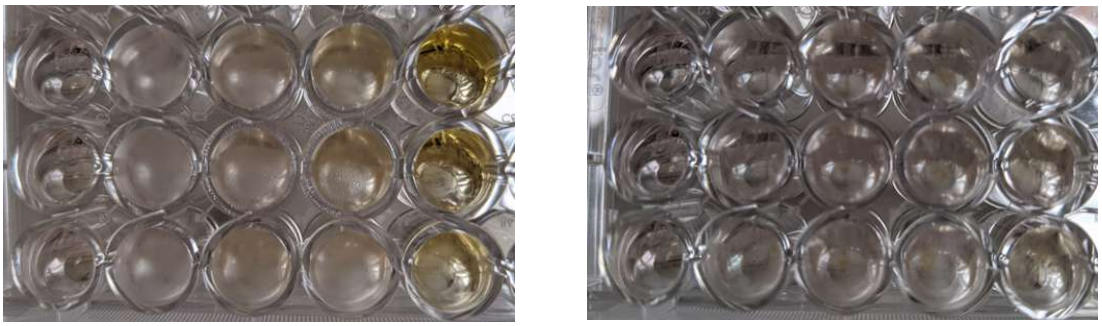

(a) **(b)**

Figure 5.6: 48-well plates containing *Aspergillus fumigatus* and *Alternaria alternata* after CAP irradiation. In (a) is shown the well plate containing *Aspergillus fumigatus* and in (b) is the well plate containing *Alternaria alternata*.

Chapter 6

Conclusion and Future Work

This multidisciplinary dissertation enabled the conjugation of fields as robotics and biology in a complementary work of Biomedical Engineering. This project had two main purposes, automatizing the pipetting technique and studying the potential of Cold Atmospheric Plasma (CAP) in antimicrobial treatment.

Regarding the automatization of the pipetting technique, the presented solution allows the laboratory operator to perform high value-added tasks while the developed system executes this repetitive technique itself, optimizing the researchers' laboratory work. Since the continuous sequence of this task, when performed manually, exposes the laboratory technicians to ergonomic hazards, this system helps to reduce the long-term impact on their musculoskeletal system.

Besides, this repetitive technique being automatized, allows a higher reproducibility due to the possibility of a constant rate of aspiration and dispensing of liquid, while the manual performance of this task can lead to human errors and low reproducibility.

The validation tests demonstrated that the developed system is able to autonomously perform the pipetting technique successfully. Therefore, the robotic system allows the researchers to improve their productivity in the working time in the laboratory, since is no longer required to manually perform the technique.

Furthermore, this project highlights the potential of the interaction between human and robot in medical environment and the fact that the robot is modular, being possible to change the end-effector according to the procedure to perform, improves its rentability and utility in clinical laboratories.

As future work, an interface could be developed to facilitate the interaction between the laboratory operator and the robotic system. This interface would allow the user to easily personalize the programming of the automatized system without being required any robotics knowledge.

Regarding the potential of CAP in antimicrobial treatment, the performed ir-

radiation assays revealed a growth inhibition in most microorganisms tested. The CAP effect was not so clear for the two yeasts tested, *Candida albicans* and *Candida parapsilosis*, and for the *Alternaria alternata* as it was for the rest of the microorganisms tested. However, the results were interesting relative to the potential of CAP as an antimicrobial treatment for the dermatophytes, *Trichophyton rubrum* and *Trichophyton mentagrophytes*, for the filamentous fungus *Aspergillus fumigatus* and for both gram-positive and gram-negative bacteria, *Staphylococcus aureus*, *Escherichia coli* and *Pseudomonas aeruginosa*.

Since *Aspergillus fumigatus* is one of the most difficult fungi that affect the human species, the CAP irradiation has to be studied in detail to be adjusted as an antimicrobial treatment to be implemented in the future. Besides, the eradication of the dermatophytes through application of CAP, which are agents of superficial infections, also present interest in medicine. Lastly, the bacteria were the microorganisms with better results since it was reached the bactericidal effect in bacteria *Pseudomonas aeruginosa* and *Staphylococcus aureus*, and a reduction of approximately 99% of the initial population of the *Escherichia coli*.

Future studies for the strains used could be performed with different times of exposure from the tested. Besides, those studies could also be performed with different microorganisms to reach a broader group of test.

Moreover, it is also important to investigate the cause of the color change of the culture medium, through the identification of the possible mechanisms responsible for that effect. Since this change was not observed in all assays and was also not immediate, being only detected after the incubation, one can conclude that the pigment production may be caused by an effect in a constituent of the culture medium or by a metabolic alteration of the microorganism. Despite these two options, it would be interesting to determine the concrete cause of this change in future work.

Furthermore, since literature has already demonstrated that the application of CAP can cause the normal cells death when a certain boundary of irradiation time is passed, it would be also interesting to study this threshold value to enable this technique as an antimicrobial treatment of wounds or infections in human tissues.

Bibliography

[1] M. Zaninotto and M. Plebani, "The "hospital central laboratory": Automation, integration and clinical usefulness," *Clinical Chemistry and Laboratory Medicine*, vol. 48, no. 7, pp. 911–917, 2010.

[2] A. S. C. P. Oliveira, "Automatizing The Application of Cold Atmospheric Plasma in Tumor Cells," Master's thesis, Universidade de Coimbra, 2019.

[3] A. Facciolà, G. F. Pellicanò, G. Visalli, I. A. Paolucci, R. Squeri, G. Nunnari, and V. L. A. Fauci, "The role of the hospital environment in the HAIs," pp. 1266–1278, 2019.

[4] S. R. Partridge, S. M. Kwong, N. Firth, and S. O. Jensen, "Mobile genetic elements associated with antimicrobial resistance," *Clinical Microbiology Reviews*, vol. 31, no. 4, pp. 1–61, 2018.

[5] J. Z. Wu, E. W. Sinsel, J. F. Shroyer, C. M. Warren, D. E. Welcome, K. D. Zhao, K.-N. An, and F. L. Buczek, "Analysis of the musculoskeletal loading of the thumb during pipetting–A pilot study," *Journal of biomechanics*, vol. 47, no. 2, pp. 392–399, 2014.

[6] N. O'Connor, O. Cahill, S. Daniels, S. Galvin, and H. Humphreys, "Cold atmospheric pressure plasma and decontamination. Can it contribute to preventing hospital-acquired infections?," *Journal of Hospital Infection*, vol. 88, no. 2, pp. 59–65, 2014.

[7] A. Kramer, I. Schwebke, and G. Kampf, "How long do nosocomial pathogens persist on inanimate surfaces? A systematic review," *BMC infectious diseases*, vol. 6, no. 1, pp. 1–8, 2006.

[8] A. Mai-Prochnow, A. B. Murphy, K. M. McLean, M. G. Kong, and K. Ostrikov, "Atmospheric pressure plasmas: Infection control and bacterial responses," *International Journal of Antimicrobial Agents*, vol. 43, no. 6, pp. 508–517, 2014.

[9] P. Zhan and W. Liu, "The changing face of dermatophytic infections worldwide," *Mycopathologia*, vol. 182, no. 1-2, pp. 77–86, 2017.

[10] R. Ben-Ami, R. E. Lewis, and D. P. Kontoyiannis, "Enemy of the (immunosuppressed) state: an update on the pathogenesis of Aspergillus fumigatus infection," *British journal of haematology*, vol. 150, no. 4, pp. 406–417, 2010.

[11] J.-P. Latgé and G. Chamilos, "Aspergillus fumigatus and Aspergillosis in 2019," *Clinical microbiology reviews*, vol. 33, no. 1, pp. e00140–18, 2019.

[12] M. Wenderoth, F. Garganese, M. Schmidt-Heydt, S. T. Soukup, A. Ippolito, S. M. Sanzani, and R. Fischer, "Alternariol as virulence and colonization factor of Alternaria alternata during plant infection," *Molecular microbiology*, vol. 112, no. 1, pp. 131–146, 2019.

[13] A. Sakudo, Y. Yagyu, and T. Onodera, "Disinfection and sterilization using plasma technology: Fundamentals and future perspectives for biological applications," *International Journal of Molecular Sciences*, vol. 20, no. 20, 2019.

[14] S. M. Al-okla, N. Salim, A. Nazwani, and F. A. Al-mudarris, "Overview of Cold Atmospheric Plasma in Wounds Treatment," *Medical Clinical Research*, vol. 5, no. 10, 2020.

[15] D. Boehm and P. Bourke, "Safety implications of plasma-induced effects in living cells - A review of in vitro and in vivo findings," *Biological Chemistry*, vol. 400, no. 1, pp. 3–17, 2018.

[16] L. Gan, S. Zhang, D. Poorun, D. Liu, X. Lu, M. He, X. Duan, and H. Chen, "Medical applications of nonthermal atmospheric pressure plasma in dermatology," *JDDG: Journal der Deutschen Dermatologischen Gesellschaft*, vol. 16, no. 1, pp. 7–13, 2017.

[17] C. A. A. Ferreira, "Plasma Frio Atmosférico Como Alternativa Terapêutica No Cancro Da Mama," 2019.

[18] D. Braný, D. Dvorská, E. Halašová, and H. Škovierová, "Cold atmospheric plasma: A powerful tool for modern medicine," *International Journal of Molecular Sciences*, vol. 21, no. 8, 2020.

[19] R. A. Felder, C. Boyd, and K. Margrey, "Robotics in the Medical Laboratory," vol. 36, no. 9, pp. 1534–1543, 1990.

[20] T. Leal Ghezzi and O. Campos Corleta, "30 Years of Robotic Surgery," *World Journal of Surgery*, vol. 40, no. 10, pp. 2550–2557, 2016.

[21] J. H. Chen and K. T. Song, "Collision-Free Motion Planning for Human-Robot Collaborative Safety under Cartesian Constraint," *Proceedings - IEEE International Conference on Robotics and Automation*, pp. 4348–4354, 2018.

[22] C. D. C. Rocha, "Sistema de bancada laboratorial para tarefas repetitivas," Master's thesis, 2016.

[23] A. L. Bailey, N. Ledeboer, and C. A. D. Burnham, "Clinical microbiology is growing up: The total laboratory automation revolution," *Clinical Chemistry*, vol. 65, no. 5, pp. 634–643, 2019.

[24] W. Gilson, "Guide to Pipetting," *Gilson guide to pipetting*, no. 3rd, pp. 1–23, 2019.

[25] Guide, "Thermo Scientific Pipetting Guide,"

[26] F. Kong, L. Yuan, Y. F. Zheng, and W. Chen, "Automatic liquid handling for life science: A critical review of the current state of the art," *Journal of Laboratory Automation*, vol. 17, no. 3, pp. 169–185, 2012.

[27] LabWrench, "Hudson robotics - solo plus." [Online], Available: https://www.labwrench.com/equipment/7382/hudson-robotics-solo-plus/, [Accessed: 05-May-2021].

[28] Biocompare, "VaryScreen I - Multi-Assay Screening System from Hudson Robotics, Inc.." [Online], Available: https://www.biocompare.com/9991-Automated-MultiPurpose-Workstations/610988-VaryScreen-I-MultiAssay-Screening-System/, [Accessed: 05-May-2021].

[29] I. Semac, G. Horak, A. Jordan, and P. Zucchelli *Andrew Alliance*.

[30] Andrew Alliance, "Better Pipetting: Better Data , Better Science," *Product Catalog*, p. 6, 2018.

[31] Labcompare, "Andrew+ Pipetting Robot from Andrew Alliance S.A.." [Online], Available: https://www.labcompare.com/313-Liquid-Handling-Robotics-Automated-Systems/14204972-Andrew-Pipetting-Robot/, [Accessed: 27-Apr-2021].

[32] K. Shaw, "Andrew Alliance CEO: In Life Science Robotics, Repeatability Is Key." [Online], Available: https://www.roboticsbusinessreview.com/health-medical/

andrew-alliance-ceo-in-life-science-robotics-repeatability-is-key/, [Accessed: 04-May-2021].

[33] Venturelab, "Exit for Andrew Alliance, the Swiss Robotic Medtech Company." [Online], Available: https://www.venturelab.ch/Exit-for-Andrew-Alliance-the-Swiss-Robotic-Medtech-Company, [Accessed: 04-May-2021].

[34] Yaskawa, "CSDA10F Dual Arm Robot for Lab Automation." [Online], Available: https://www.yaskawa.eu.com/products/robots/handling-mounting/productdetail/product/csda10f_712, [Accessed: 30-June-2021].

[35] Yaskawa Europe, "Flexible Lab Automation with robot MOTOMAN CSDA10F," *Flyer Robot CSDA10F*, pp. 10–13, 2017.

[36] Y. Bar-Cohen, "Introduction to Biomimetics: The Wealth of Inventions in Nature as an Inspiration for Human Innovation," in *Biomimetics: biologically inspired technologies*, CRC Press, 2005.

[37] F. Wang, M. Nan, S. Cho, C. S. Kim, J. O. Park, and E. Choi, "Bioinspired Ionic Soft Actuator Based on Core-Shell-Structured Bacterial Cellulose Membrane," *MARSS 2018 - International Conference on Manipulation, Automation and Robotics at Small Scales*, pp. 1–4, 2018.

[38] P. Sandin, *Robot mechanisms and mechanical devices illustrated*. McGraw Hill Professional, 2003.

[39] S. Nagai and A. Kawamura, "Position Sensorless Position Control for Dual Solenoid Actuator," *2018 International Power Electronics Conference, IPEC-Niigata - ECCE Asia 2018*, pp. 1687–1691, 2018.

[40] P. I. Philatenkov, E. V. Morozova, and T. S. Morozova, "Linear Actuator Modeling," *Proceedings of the 2020 IEEE Conference of Russian Young Researchers in Electrical and Electronic Engineering, EIConRus 2020*, pp. 807–809, 2020.

[41] S. Joshi and J. Paik, "Pneumatic supply system parameter optimization for soft actuators," *Soft Robotics*, 2020.

[42] MFE 3004, "Actuation in mechatronic systems."

[43] J.-a. Epinette and K. Sutton, "User's Guide," no. November, pp. 1–44, 2003.

[44] Gilson, "PIPETMAN Classic P100." [Online], Available: https://pt.gilson.com/pipetman-classic-p100.html, [Accessed: 01-June-2021].

[45] ROBOTIS, "XL430-W250-T." [Online], Available: https://emanual.robotis.com/docs/en/dxl/x/xl430-w250/, [Accessed: 15-June-2021].

[46] ROBOTIS, "DYNAMIXEL XL430-W250-T." [Online], Available: https://www.robotis.us/dynamixel-xl430-w250-t/, [Accessed: 15-June-2021].

[47] R. V. Petrescu, R. Aversa, B. Akash, R. Bucinell, J. Corchado, A. Apicella, and F. I. Petrescu, "Gears-Part I," *American Journal of Engineering and Applied Sciences*, vol. 10, no. 2, pp. 457–472, 2017.

[48] Autodesk Knowledge Network, "Spur Gears Component Generator dialog box - Design tab." [Online], Available: https://knowledge.autodesk.com/support/inventor/learn-explore/caas/CloudHelp/cloudhelp/2021/ENU/Inventor-Help/files/GUID-3BCB80E6-3328-433B-972D-C92D6CED7674-htm.html, [Accessed: 22-September-2021].

[49] Prusa Knowledge Base, "PLA." [Online], Available: https://help.prusa3d.com/en/article/pla_2062, [Accessed: 26-September-2021].

[50] P. M. Matos, "Collaborative Gripper for Robotic Applications," Master's thesis, Universidade de Coimbra, 2019.

[51] Arduino Official Store, "Arduino Uno Rev3." [Online], Available: https://store.arduino.cc/products/arduino-uno-rev3, [Accessed: 30-October-2021].

[52] Robotis, "DYNAMIXEL Shield." [Online], Available: https://www.robotis.us/dynamixel-shield/, [Accessed: 30-October-2021].